Space-time data-driven modeling of wildfire initiation in the mountainous region of Trentino–South Tyrol, Italy

Mateo Moreno[1*], Stefan Steger[2], Laura Bozzoli[3, 4], Stefano Terzi[3], Andrea Trucchia[5], Cees van Westen[1] and Luigi Lombardo[1]

Abstract

Wildfires are complex hazards occurring worldwide, leading to substantial economic losses, fatalities, and carbon emissions. The interplay of climate change, land use alterations, and socioeconomic pressures is expected to further increase the frequency and intensity of wildfires. In this context, developing reliable, dynamic prediction tools is essential for risk mitigation. This work presents a spatiotemporal wildfire prediction model for the Trentino-South Tyrol region (13,600 km^2) in the northeastern Italian Alps. Leveraging generalized additive models, we integrate multitemporal wildfire records (2000–2023) with static and dynamic environmental controls (e.g., topography, land cover, daily precipitation, and temperature). The resulting model predictions change dynamically over space and time in response to static features, seasonal trends, and evolving meteorological conditions. Model outputs were evaluated using established performance metrics, enabling the derivation of dynamic spatial wildfire probability thresholds. These thresholds are illustrated for varying amounts of precipitation, temperature, and different combinations of static factors. Validation through multiple perspectives yielded performance scores generally exceeding 0.8, confirming the model strong generalization and transferability. To demonstrate the practical application, the model was used to hindcast past wildfire initiation between 1–15 July 2022–a period marked by elevated wildfire activity. By integrating static and dynamic environmental controls, this research advances the spatiotemporal prediction of wildfires in complex alpine regions, supporting the development of early warning systems.

Keywords: Early warning; Space-time modeling; GAMs; Dynamic wildfire forecasting; Wildfire ignition

[1]University of Twente, Enschede, The Netherlands
[2]GeoSphere Austria, Vienna, Austria
[3]Eurac Research, Bolzano, Italy
[4]University of Trento, Trento, Italy
[5]CIMA Research Foundation, Savona, Italy

1 Introduction

Wildfires are frequent hazards posing significant threats to society and the environment. On average, an estimated 350 Mha burns globally each year (Giglio et al., 2013). The economic toll of wildfires is severe, with global wildfire-related losses amounting to approximately USD$142 billion since 2000, as reported by the international disaster database (EM-DAT; Jones et al., 2022). Some of the most devastating wildfires in recent history include the events in Australia, the United States, and Chile (Filkov et al., 2020; Maranghides et al., 2023; Guerrero et al., 2024). Beyond their immediate economic and societal consequences, wildfires are a major source of carbon emissions, releasing an estimated 2–3 billion tons of CO_2 annually, at times surpassing 50% of emissions from fossil fuel combustion (Jolly et al., 2015; van der Werf et al., 2017). Their impacts manifest across multiple scales as locally, wildfires disrupt ecosystems, threaten human settlements, and damage infrastructure (Driscoll et al., 2024); regionally, they accelerate soil erosion, reducing agricultural productivity (Keeley et al., 2017); and globally, their carbon emissions contribute to climate change, potentially amplifying future wildfire risk (Zscheischler et al., 2018). Given the severe impacts of wildfires, there is an increasing need to minimize their harm and, as such, the ability to ensure operational preparedness. In this context, reliable wildfire predictions and developing wildfire early warning systems (WEWS) are essential for reducing wildfire impacts and improving response efforts.

Wildfires occur when an ignition source interacts with available fuel under suitable weather conditions, with subsequent behavior often influenced by terrain. Like other natural hazards, wildfires are governed by multiple controls across various spatiotemporal scales. At the smallest scale, fire behavior is commonly described by the "fire triangle" concept (Countryman, 1972; Pyne et al., 1996), identifying heat, fuel, and oxygen as the three fundamental components necessary for combustion. At the scale of a single wildfire, its occurrence and propagation are driven by a complex interplay of static and dynamic environmental controls (Moritz et al., 2005). Static factors such as the topography, hydroclimatic predisposition, and vegetation (fuel type) can determine whether an area is prone to wildfires or the "where" (Faivre et al., 2014). In contrast, the timing, or the "when", is governed by dynamic controls such as air temperature, precipitation, fuel moisture, and anthropogenic influences—including arson or accidental ignitions—which directly affect ignition likelihood and fire spread (Bessie et al., 1995; Ganteaume et al., 2013). Therefore, assessing "where" and "when" wildfires may occur requires a comprehensive evaluation of static and dynamic factors influencing wildfire behavior (Finney, 2005; Koutsias et al., 2015).

In this context, data-driven models are widely used to assess wildfire occurrence over large areas (Martínez et al., 2009; Cao et al., 2013; Ghorbanzadeh et al., 2019; Tonini et al., 2020; Bjånes et al., 2021; Trucchia et al., 2022b; Yue et al., 2023). Despite its widespread use in fire prediction, the concept of susceptibility has been defined in various ways (Verde et al., 2010; Cao et al., 2017; Leuenberger et al., 2018). In this contribution, we adopt a definition analogous to that used for landslides and in agreement with Leuenberger et al. (2018), describing wildfire susceptibility as the likelihood of a fire occurring within a given spatial unit (e.g., grid cells, catchments, administrative units) based on local predisposing factors. In other words, it predicts "where" wildfires will likely occur (Brabb, 1984;

Guzzetti et al., 2005). In a purely spatial context, data-driven models derive statistical relationships between historical records of wildfire occurrence, i.e., wildfire inventories, as static environmental factors to estimate wildfire susceptibility (Arndt et al., 2013; Oliveira et al., 2012; Trucchia et al., 2022a; Zhang et al., 2021). Placing the spotlight on the spatial domain, wildfire susceptibility assessments provide valuable insights to support fire management, whether as standalone analyses or as part of broader risk assessment frameworks and spatial planning strategies (Oliveira et al., 2021; Jappiot et al., 2009; Chuvieco et al., 2010; Sebastián-López et al., 2008). Nevertheless, these approaches often disregard the temporal component, excluding the assessment of critical meteorological conditions that influence wildfire occurrence.

The temporal component of wildfire prediction is usually assessed through dynamic factors, primarily focusing on daily variations in meteorological conditions, which form the foundation of traditional WEWS (Chuvieco et al., 2010) and serve as tools for defining local fuel treatments, surveillance, and suppression activities (Ager et al., 2010; Scott et al., 2012; Oliveira et al., 2021). Numerous largely empirical wildfire danger indices, also called fire danger rating systems, are used worldwide. A comprehensive literature review of these index-based rating systems is beyond the scope of this contribution and can be found in Viegas et al. (1999); Chuvieco et al. (2003); Arpaci et al. (2013); Giuseppe et al. (2016); Pérez-Sánchez et al. (2017); Sirca et al. (2018); Pagnon Eriksson et al. (2023). Wildfire danger indices empirically quantify the relative wildfire danger in a given area based on meteorological conditions. Notable examples include the Canadian fire weather index (FWI; Wagner et al., 1987), which relies on meteorological input data—wind speed, air temperature, relative humidity, and precipitation—to assess daily wildfire danger. Although initially developed for pine fuel types prevalent in Canadian forests, the FWI has been extensively tested worldwide (Kudláčková et al., 2024). Similarly, the McArthur's forest danger index (FDI; Noble et al., 1980; Hollis et al., 2024) was developed to evaluate wildfire danger and behavior in Australian eucalyptus forests, incorporating fuel availability implicitly through atmospheric conditions. Another example is the Italian index IREPI (Bovio et al., 1984), designed to assess wildfire danger during the winter–spring season in northwestern Italy, which accounts for soil water loss due to evapotranspiration derived from the multiple meteorological input data. Despite the utility of this fire danger system and its spatially explicit features, these rating systems often overlook factors such as intrinsic terrain characteristics, seasonality, and human influences, both of which are critical in wildfire ignition and propagation (Chuvieco et al., 2010).

The integration of the spatial and temporal components for wildfire prediction in large areas remains challenging. However, existing studies underscore its considerable potential. For instance, de Santana et al. (2021) modeled the occurrence of wildfires over a 19-year period by integrating static and dynamic predictors aggregated on an annual scale, generating independent susceptibility maps for each year. In Verde et al. (2010); Parente et al. (2016); Oliveira et al. (2021), the wildfire hazard was estimated by combining the static wildfire susceptibility with a probabilistic assessment of wildfire recurrence, based on projected future burned areas within each mapping unit. Bergonse et al. (2021) integrated wildfire susceptibility with a meteorological index representing spring conditions, enabling predictions for any given year before the critical fire season. Conversely, Deng et al. (2023) used a deep learning approach to predict daily wildfire ignition scores by integrating dynamic weather predictors—such as temperature, rainfall, humidity, and wind—with static factors. Richards et al. (2023) leveraged a spatiotemporal interpretable neural network to model both wildfire ignition and spread, incorporating both static and dynamic factors at a monthly resolution over the period 2001–2020. Woolford et al. (2011) employed generalized additive models (GAMs) to predict wildfire occurrence during the active fire season over a 24-year period, integrating both static and dynamic factors. Their study emphasized the high interpretability of the chosen approach and the influence of anthropogenic predictors, such as population density and proximity to infrastructure.

In the Alpine context, wildfires pose a significant threat to mountain forests and their protective function against other natural hazards such as rockfalls, avalanches, mudflows, increased run-off, and soil erosion (Maringer et al., 2016; Martin et al., 2001; Robichaud et al., 2006). The region is characterized by two main fire seasons: an early spring peak in March or April, driven by frost-induced dryness, and a summer peak in July and August due to high temperatures (Müller et al., 2020a). To support wildfire assessment and forest protection, multiple WEWS have been developed across different Alpine countries. For instance, the European forest fire information system (EFFIS; Giuseppe et al., 2016) provides large-scale fire danger assessments at a spatial resolution of 8×8 km, but its applicability in complex Alpine terrain is limited. National-level models, such as the one in Austria, achieve resolutions of 1×1 km using meteorological inputs from weather forecasting systems like INCA (Haiden et al., 2011), although a more recent prototype was developed, achieving a spatial resolution of 100×100 m (Müller et al., 2020b). Despite these efforts, wildfires in the Alps remain a significant challenge. In Italy, the average Alpine wildfire covers about one hectare, but 10% of the fires exceed 10 ha, accounting for 85% of the total burned area (Müller et al., 2020a). Human activities are the primary cause of ignitions, responsible for about 90% of ignitions, though lightning-induced fires can contribute up to 50% of ignitions in some areas during the summer season (Müller et al., 2013). Advancements in WEWS have brought improvements, yet the spatial resolution of existing models might be insufficient to capture the complex interactions between wildfire behavior and the heterogeneous Alpine topography, including narrow valleys, mountain peaks, high-altitude plateaus, and their effects on weather controls (Carrega, 1995; Schunk et al., 2013; Müller et al., 2020b). As wildfire frequency and severity are expected to rise, there is a growing need for high-resolution fire prediction models that integrate both static and dynamic factors to enhance preparedness and mitigation strategies (Chuvieco et al., 2010; Wastl et al., 2012).

This study investigates space-time wildfire initiation modeling by adapting a previously developed framework devised for the assessment of mass movement hazards in an Alpine region of northern Italy (Steger et al., 2023; Moreno et al., 2024; Steger et al., 2024; Moreno et al., 2025). Following a similar modeling approach, we aim to integrate static and dynamic wildfire controls using data-driven techniques to estimate wildfire initiation probabilities in space and time. Furthermore, we aim to enhance the applicability of the model by linking the predicted probabilities to quantitative thresholds. These analyses are performed for the region of Trentino–South Tyrol (Italy), covering a period of 24 years (2000–2023).

The remainder of this paper is structured as follows: Section 2 describes the study area and its environmental characteristics. Section 3 introduces the wildfire historical records and the different static and dynamic factors used in the modeling. Section 4 details the methods, including the sampling procedure, data extraction, modeling with GAMs, validation strategies, and the thresholding approach. Section 5 presents the key results, emphasizing data sampling, model interpretation, and application. Ultimately, Sections 6 and 7 discuss the findings and conclude with an outlook on future research directions.

2 Study area

Our study area (shown in Figure 1) corresponds to the upper Adige River Basin, encompassing the region of Trentino-South Tyrol in the northeastern Italian Alps, covering an area of about 13,600 km^2. Its diversified landscape and climatic conditions characterize the region. The mountainous topography is dominated by pronounced variations in elevation, ranging between ~65 m a.s.l. (above sea level) in the southernmost part of the region, close to Lake Garda to ~3900 m a.s.l. at the Ortles peak in the northwest. Due to physiographical features, Trentino-South Tyrol is highly prone to various mountain-related natural hazards, including avalanches, rockfalls, and mudflows. Due to the proximity of human settlements to the steep Alpine terrain, a significant portion of the infrastructure is exposed to these processes.

The interaction of humid air masses from the northwest Atlantic, warm Mediterranean influences, and dry continental air from the east shapes the regional climate. This intersection gives rise to a pronounced seasonal cycle characterized by warm and humid summers and cold and dry winters (Norbiato et al., 2009; Adler et al., 2015). The complex interplay of topography and diverse atmospheric conditions of the region determines the strong seasonality and spatial variations in precipitation and temperature. The annual precipitation sum varies significantly across the region, ranging from ~500 mm in the northwestern rain-shaded inner valleys to over 1,700 mm in the southeastern parts, maintaining a spatial average over the study area of about 1000 mm. Similarly, mean annual temperature varies substantially, from approximately +14°C in the Garda Valley to around −11°C at the Ortles peak, with an overall regional average of about +5°C. The annual cycles of precipitation and temperature are characterized by the warmest and wettest conditions during summer (July–August) and the coldest and driest conditions towards the late winter (January–February). The most significant warming and precipitation increase occurs towards spring (April–May; Crespi et al., 2021).

The land cover in the region is predominantly forest (~45%), primarily consisting of coniferous trees located on hillsides. Herbaceous vegetation and heathland account for ~35%, while cultivated land, mainly concentrated in the valley bottoms, represents ~8%. The remaining land cover includes mostly rocky outcrops, water bodies, permanent snow-covered surfaces, and urban areas.

3 Data

3.1 Wildfire database

The wildfire inventory for the region was obtained from the Forestry Service Department (Abteilung Forstdienst/Ripartizione Servizio Forestale) of South Tyrol and the Forestry and Wildlife Service of Trentino (Servizio Foreste e Fauna). The databases were accessed in early 2024; the former was directly provided by the office in charge, and the latter can be accessed at https://siat.provincia.tn.it/geonetwork/srv/ita/catalog.

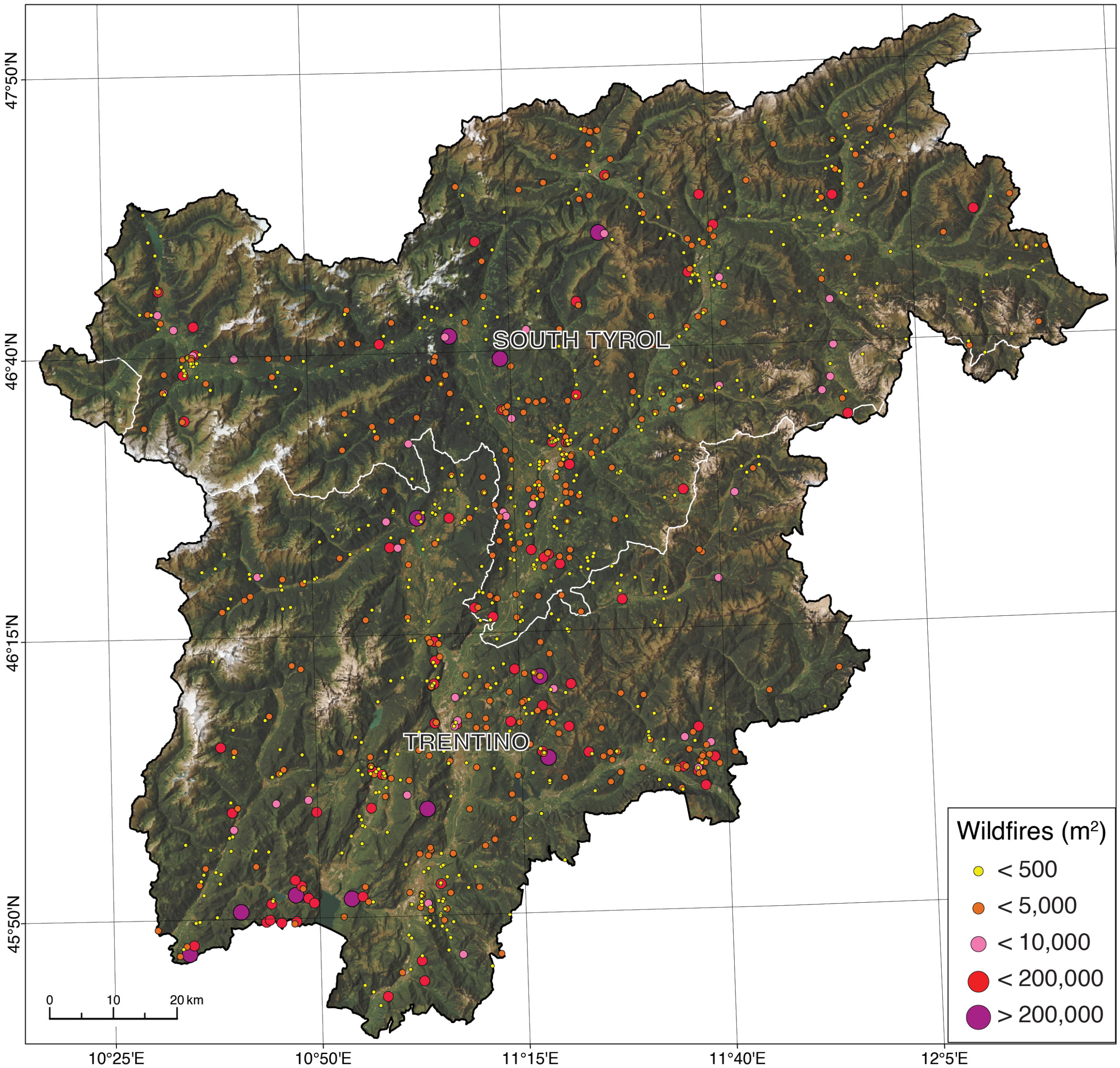

Figure 1: Study area showing the spatial distribution of wildfire centroids (n = 998) across the Trentino–South Tyrol region, with symbol size and color representing the respective burned area for each event. Basemap imagery courtesy of Earthstar Geographics.

The wildfire inventory of South Tyrol is divided into two periods: records from 1999 to 2017 and those from 2017 onward. This distinction reflects changes in mapping techniques, as polygonal representations of burned areas were introduced only after 2017. Before this, fire locations were recorded as points, presumably indicating a location within the affected area. The dataset includes 608 wildfire events with attributes such as date and time of occurrence, duration, total burned area, and causes.

Similarly, the wildfire inventory of Trentino is structured into two periods: records from 1966 to 1983 and those from 1984 onward. The earlier dataset comprises 1,062 events, where only the burned area polygons were documented, without associated timestamps and other relevant attributes. From 1984 onward, the dataset includes 3,134 wildfire events, with temporal resolution improving over time. While timestamps were recorded at the yearly level until 2007, only 507 events after 2007 include precise day-of-occurrence information, leaving 2,627 with year-only time stamps. The recorded attributes in this dataset include the occurrence time (with varying temporal resolution), total burned area, and forested burned area.

Since the main objective of this study is to predict wildfire occurrence in space and time, the analyses focus on wildfire events for which occurrence dates are available. Only these events were extracted from the inventories to ensure the desired temporal resolution in the modeling. Further details on this methodical step are provided in Section 4.1.

3.2 Environmental factors

Static factors

Identifying wildfire-prone areas using data-driven approaches relies on analyzing spatial environmental factors observed at locations with and without wildfire occurrences. The choice of predictors was guided by the numerous contributions that have explored the influence of different static factors and their role in wildfire modeling (Ganteaume et al., 2013; Jain et al., 2020). For this case study, we prioritized predictors that offer meaningful insights into wildfire occurrence.

We used the NASADEM (NASA JPL, 2020) to derive standard morphological factors such as *slope steepness*, which may facilitate fire spread (Chuvieco et al., 2010), and *aspect*—decomposed into the components *eastness* and *northness*—to capture variations in solar exposure and moisture retention (Müller et al., 2020b). A proxy for vegetation and fuel types was represented using data extracted from the CORINE land cover and high-resolution map of Europe 2017 (Malinowski et al., 2020). The data were subsequently reclassified into eight categories: (*i*) *artificial surfaces*, (*ii*) *agricultural land*, (*iii*) *broadleaf tree cover*, (*iv*) *coniferous tree cover*, (*v*) *herbaceous vegetation and heathland*, (*vi*) *marshes and peatbogs*, (*vii*) *natural material surfaces*, and (*viii*) *permanent snow-covered surfaces and water bodies*. To further characterize vegetation within forested areas and measure forest structure, we utilized the *tree cover density* dataset extracted from European Union's Copernicus Land Monitoring Service information (2020). Climatic predisposition predictors, including *total annual precipitation* and *mean annual temperature*, averaged over a 30-year period from 1981 to 2010, were also tested to characterize the regional climate and its influence on wildfire occurrence (Crespi et al., 2020). Finally, to account for the anthropogenic component and infrastructure, buildings and roads were extracted from OpenStreetMap (OSM;

OpenStreetMap contributors, 2017). The Euclidean *distance to buildings* and *roads* were then computed to incorporate their effects on wildfire modeling. All the environmental factors were resampled to a 50 m spatial resolution for modeling purposes.

Dynamic factors–gridded precipitation and temperature fields

We used the high-resolution gridded daily temperature and precipitation dataset for Trentino–South Tyrol provided in Crespi et al. (2021). The dataset was built upon a dense network of over 200 meteorological stations, ensuring comprehensive coverage across the study area. Initially, the data processing involved multiple methodical steps, including quality and consistency checks, homogeneity tests, and gap-filling techniques to maximize data completeness. Using the processed database, an anomaly-based interpolation scheme was applied to project the daily fields of precipitation and mean temperature onto a grid of 250 m resolution. The accuracy, estimated via leave-one-out cross-validation, yielded a mean absolute error (MAE) of 1.1 mm for precipitation and 1.5°C for mean temperature, averaged across all stations and months. For each day, the dataset provides the total precipitation accumulated over 24 hours, from 08:00 UTC of the previous day to 08:00 UTC of the observation day, and the daily mean temperature is defined as the average of the daily maximum and minimum temperature.

4 Method

The method implemented in this research extends a data-driven framework initially devised for the assessment of mass movement hazards (Steger et al., 2023; Moreno et al., 2024; Steger et al., 2024; Moreno et al., 2025), adapting it to integrate static and dynamic wildfire controls for estimating wildfire occurrence probabilities in space and time. The workflow comprises five main steps: (*i*) *filtering and sampling rulesets*. Since our model is based on binary data, we first need to define our target variable: the areas with wildfire occurrence or wildfire presences and those without or wildfire absences. First, we defined the wildfire presences by combining the different wildfire databases and filtering the individual records based on the inventory attributes. This is followed by the definition of wildfire absences, where we applied a strategic sampling procedure to define wildfire absences, considering both spatial and temporal aspects. The subsequent (*ii*) *data extraction–precipitation and temperature time windows* phase retrieves static and dynamic predictors, with dynamic predictors grouped into time windows. In (*iii*) *modeling and grid search*, we implement a binomial GAM to perform a grid search and select the optimal combination of cumulative precipitation and temperature to describe wildfire occurrence, which is then integrated with static predictors to fit the final spatiotemporal model. (*iv*) *Model evaluation* follows, incorporating plausibility checks and cross-validation routines from multiple perspectives to assess predictive performance. Finally, the predictions are linked to quantitative metrics, facilitating (*v*) *visualization and thresholding*, with a hindcasting example provided to demonstrate model applicability.

4.1 Filtering and sampling rulesets

Wildfire presences

The four wildfire inventories—two from South Tyrol and two from Trentino—were preprocessed before being integrated into a single dataset. For South Tyrol, we used only the point-based wildfire records. These records initially spanned the period from 1999 to 2017 but remained consistently available through 2023. Although polygon-based records were available after 2017, they were excluded while point-based records were retained to ensure spatial consistency, as comparisons between points and polygons did not always follow a clear pattern. Since our analysis period starts in the year 2000, any events occurring before this year were removed, resulting in the filtered wildfire dataset for South Tyrol.

Since our model aims to predict wildfire occurrence on a daily scale, only wildfire records with an associated daily timestamp were considered. In the case of Trentino, this requirement led to the selection of the inventory covering the period from 1984 onward, while records from earlier periods, without any timestamp, were excluded. Additionally, wildfire events lacking a recorded *day of occurrence* (i.e., those before 2007) were removed. To ensure a uniform spatial representation across the inventories in South Tyrol and Trentino, wildfire occurrences in Trentino were represented as point centroids of their respective burned area polygons.

The two inventories were merged into a single dataset, forming the preliminary wildfire sample. Events with a *burned area* smaller than 10 m^2 were filtered out to ensure data reliability, resulting in a final dataset for the subsequent analysis. Finally, for data extraction, we consider a buffer of 50 m around each point to enhance the spatial representativeness of each wildfire point.

Wildfire absences

Selecting wildfire absence data is just as crucial as the wildfire presence filtering. However, defining the absences poses a greater challenge, as it requires identifying not only location but time periods where wildfires are unlikely to have occurred. The sampling strategy is essential in shaping the model structure and is directly reflected in the modeling outcomes. Therefore, ensuring a well-balanced representation across spatial and temporal domains is essential to prevent wrongly estimated model relationships and potentially biased predictions. To this aim, we considered several rules, including (i) masking out trivial terrains, (ii) implementing temporal buffers, (iii) balancing samples across years and months, and (iv) masking out trivial periods that are detailed below.

Trivial terrains are locations where wildfire initiation is not expected. In our analysis, we defined these areas based on the available fuel that can be accounted for using the land cover map. In this way, the classes referring to *artificial surfaces*, *natural material surfaces* (*e.g., bare rock, sand*), and *permanent snow-covered areas and water bodies* were excluded from the spatial domain as there is no fuel to be potentially burned. This resulted in a mask being used to sample space wildfire absence locations. Notably, no recorded wildfire events were located within trivial terrains.

Wildfire absences were sampled under two different schemes, including the sampling of wildfire absences at presence locations and the sampling of wildfire absences at absence locations. For the first scheme, wildfire absences at presence locations were generated by replicating records from the filtered wildfire inventory and assigning a random observation date within the period of analysis, i.e., 01-01-2000 to 31-12-2023. To ensure that the selected dates were temporally meaningful, a temporal buffer was applied to avoid selecting dates within five years of the respective wildfire occurrence. This step aimed to allow sufficient time for vegetation (fuel) recovery before it may be subject to wildfire occurrence, as supported in Sass et al. (2017), Bowd et al. (2021), and Mantero et al. (2023). A 30-day temporal buffer was also introduced to avoid overlapping meteorological information when extracting the dynamic predictors, as explained in Section 4.2.

For the second scheme, wildfire absences at absence locations were generated by randomly sampling absence locations, excluding the trivial terrains and the areas that had been burned before, according to the filtered inventory. Once absence locations were identified, they were replicated and assigned a random observation date for the specified analysis period (01-01-2000 to 31-12-2023). Similar to the first scheme, the date selection was constrained by a 30-day temporal buffer to avoid overlapping meteorological data.

The preliminary wildfire absence subset was formed by combining the wildfire absences at presence locations and those at absence locations. Subsequently, the absence subset was further refined by balancing the observation dates across the different years and months to achieve a uniform temporal representation. The results of this step were combined with the wildfire presences to obtain the modeling sample, which was subjected to a final filtering step to account for trivial periods, as described in Section 4.2.

4.2 Data extraction–precipitation and temperature time windows

The static predictors were extracted to the modeling sample using the datasets described in Section 3. Additionally, predictors regarding the occurrence date, specifically *year*, *month*, and *day of the year* (*doy*) were derived from the assigned observed date in the modeling sample. Data extraction was performed for the meteorological predictors such as precipitation and temperature by linking each sample location and date to the high-resolution gridded dataset from Crespi et al. (2021). Both predictors were retrieved up to 30 days before the assigned observation date. Similar to trivial terrains, we defined trivial periods based on a precipitation threshold so that observations with precipitation amounts ≥1.1 mm on the day of observation were excluded from the analysis. This filtering step was necessary because including large amounts of "wet" days—presumably with no wildfire occurrence—into the binary classification model would result in the model simply learning the difference between "dry" and "wet" conditions. Hence, we applied the precipitation threshold to explicitly keep the modeling target to predict wildfire occurrence in "dry" periods.

Finally, the precipitation and temperature predictors were structured into multiple time windows for analysis. The predictor P represents the cumulative precipitation within a given time window, while Te corresponds to the mean daily temperature over the same period. As an analogy to what was described in Steger et al. (2023), P aims to represent the medium-term preparatory precipitation, which can be seen as a proxy for the surface moisture conditions, whereas Te can be seen as the short-term temperature. This approach enabled a systematic evaluation of how the combination of different antecedent precipitation and temperature influences wildfire occurrence.

4.3 Modeling using GAMs and grid search

Theoretical background

Generalized additive models are semi-parametric regression models that extend generalized linear models (GLMs) by incorporating additive smooth functions to capture nonlinear relationships between predictor variables and the response (Wood, 2006; Bolker et al., 2009; Zuur et al., 2009). In this study, the binary response variable, representing wildfire presence or absence, follows a Bernoulli probability distribution and can be generically expressed as:

$$\text{logit}(p_i) = \beta_0 + f_1(x_{1i}) + f_2(x_{2i}) + \dots + f_n(x_{ni}) \quad (1)$$

Where f_1, f_2 and f_n are smooth functions to model the nonlinear effects on each of the predictors x_{1i}, x_{2i}, and x_{3i}. A logistic link function is applied to relate p_i to the effects of the predictor variables. Due to their high interpretability and flexibility—often described in the literature as *white-box models*—GAMs have been extensively used across various disciplines, including natural hazard modeling (Woolford et al., 2011; Pourtaghi et al., 2016; Ríos-Pena et al., 2017; Lombardo et al., 2020; Eskandari et al., 2021; Opitz et al., 2022; Moreno et al., 2023; Alvioli et al., 2024).

Grid search and model fit

In this contribution, GAMs were applied in two distinct phases: (i) to identify the optimal time windows *P* and *Te* that best describe wildfire initiation, and (ii) to integrate static factors with the identified best *P* and *Te* windows to estimate wildfire probabilities in space and time. The analyses were conducted using the comprehensive R package *mgcv* (version 1.9-1; Wood, 2017).

The selection of optimal time windows for *P* and *Te* was conducted through a systematic grid search. This procedure involved a pairwise comparison of different *P* and *Te* time window combinations using a binomial GAM. This model was fitted to the previously defined modeling sample, as explained in 4.1, incorporating iteratively the different combinations of *P* and *Te*, and the *doy* as predictors. The grid search evaluated 30 time windows for *P* and 10 for *Te*, resulting in 300 unique combinations. Each combination underwent a 10-fold random cross-validation with 10 repetitions to ensure robustness, yielding 300,000 iterations. The performance of the model was recorded for each iteration—based on well-known performance metrics addressed in Section 4.4—allowing for a systematic comparison to identify the optimal pair of time windows that best describe wildfire initiation.

The selected optimal time windows *P* and *Te* were integrated with the static predictors to develop the spatiotemporal wildfire initiation model. The model fitting process was iterative, starting with a simple baseline configuration and progressively incorporating additional predictors. Each newly introduced predictor was assessed by visually inspecting partial effect plots and formally inspecting p-values, confidence intervals, and the overall model fitting performance. Once the final model fit was obtained, the relative contribution of each predictor was evaluated using a permutation-based variable importance analysis. This assessment indicates how much each predictor contributes to the model by randomly permuting its values and measuring the resulting change in the model prediction error.

Specifically, the analysis was based on the deviance explained—a widely used measure of goodness of fit derived from the likelihood function. The importance of each predictor was quantified by comparing the deviance explained by the final model fit against a series of models, each with a single predictor permuted. These permutations disrupt the original relationship between the predictor and the response; therefore, a greater reduction in the deviance explained indicates a more substantial contribution of each permuted predictor (Schlögl et al., 2025). In this study, permutation feature importance was summarized using the mean and standard deviation to quantify both the average effect and the associated uncertainty. For the interpretation and plausibility of the model relationships, partial effect plots were generated, illustrating how individual predictors influence wildfire occurrence probabilities while holding all other predictors constant at their average values. Additionally, interaction effects between predictors were visualized using contour plots, providing further insights into the complex relationships governing wildfire dynamics.

4.4 Model evaluation

For a comprehensive evaluation of the model performance, we leveraged multiple validation strategies using the R package *sperrorest* (version 3.0.5; Brenning, 2012). The assessment included k-fold random cross-validation (RCV), k-fold spatial cross-validation (SCV), temporal cross-validation (TCV) based on years and months, and leave-one-factor-out cross-validation (FCV) using the land cover data. These approaches ensured a robust model generalization and transferability assessment across different spatial, temporal, and environmental conditions.

Random cross-validation was implemented by partitioning the dataset into independent training and testing sets. We applied a ten-fold RCV with ten repetitions, resulting in 100 iterations (Brenning, 2012). While RCV provides a general measure of model predictive performance, it may overlook spatial heterogeneity, potentially leading to over-optimistic results if the model performs inconsistently across different subregions. To address this, we incorporated SCV, which estimates the spatial transferability of the model by evaluating its performance in spatially distinct partitions. The spatial partitioning was achieved using a k-means clustering approach, ensuring alignment with the ten-fold, ten-repetition setup used in RCV.

To further assess model generalization and transferability, we applied TCV and FCV. The former was conducted by iteratively excluding wildfire observations from either one month (leave-one-month-out) or one year (leave-one-year-out) and then evaluating model predictions on the omitted data. This approach allowed us to test how well the model performs when transferred to unseen time periods at the scale of years and months. Similarly, FCV was performed using the five nontrivial land cover classes—*agricultural land, broadleaf tree cover, coniferous tree cover, herbaceous vegetation, and heathland,* and *marshes and peatbogs*— to define independent training and testing datasets, ensuring that the model performance was not overly dependent on specific land cover conditions.

The model performance for each validation approach was quantified using the area under the receiver operating characteristic curve (AUROC) computed for independent testing sets. The ROC curve represents the classifier performance across varying cut-off thresholds, with AUROCS values ranging from 0.5, i.e., random classification to 1, i.e., perfect discrimination (Hosmer et al., 2013). Higher AUROC values indicated stronger performance, providing an objective measure to compare different validation strategies and assess the model robustness across spatial, temporal, and land cover variations.

4.5 Thresholding and visualization

In this research, we adapted an extension of empirical rainfall thresholds—–traditionally employed in landslide early warning systems(Brunetti et al., 2010)—–to wildfire prediction. Conventional landslides thresholds operate on the premise that slope failures become probable when specific rainfall parameters exceed critical values. Recent advancements in Steger et al. (2024) showed that spatial dynamic landslide probability thresholds can be derived by incorporating both dynamic meteorological controls and static terrain conditions. Building upon this methodological framework, we developed analogous spatially explicit thresholds for wildfire prediction, enabling the reclassification of dynamic probability maps to directly visualize threshold exceedance patterns across varying spatiotemporal contexts.

In our wildfire analysis, we employ heatmap visualizations to represent wildfire probability scores for increasing amounts of the meteorological predictors P and Te. To enhance the practical application of this results, we established three distinct threshold derived from the ROC curve, transforming the continuous probability scores (0–1) into meaningful discrete classes. These thresholds represent specific combinations between correctly classified wildfires (true positive rate or sensitivity; *TPR*) and wrongly classified absences (false alarms or false positive rate; *FPR*), thereby providing a more nuanced categorizations of wildfire likelihood. The *TPR95* threshold establishes a high sensitivity benchmark, ensuring that 95% of observed wildfires occur in areas and periods exceeding this probability value. While this threshold effectively captures most wildfire-prone conditions, it comes at the expense of generating a high proportion of false alarms. On the other hand, the *TPR35* threshold implements a more stringent criterion, identifying only 35% of wildfire occurrences. This higher-probability threshold substantially reduces false alarms but excludes 65% of actual wildfire events, capturing only the most extreme wildfire-prone conditions.

Positioned between these two extremes, we implemented an optimal *OPT* threshold based on the Youden index, which maximizes the sum of correctly classified wildfire and non-wildfire locations and periods. This threshold corresponds to the point on the ROC curve with maximum vertical distance from the diagonal line representing a random classification (Fluss et al., 2005; Ruopp et al., 2008). The *OPT* threshold provides the most balanced compromise between the classification of wildfire and non-wildfire conditions. Utilizing these three thresholds, our final dynamic probability map delineates four distinct wildfire likelihood classes, with *OPT* as the central reference point.

The resulting dynamic maps directly visualize wildfire threshold exceedance across the study region. To further evaluate the practical utility of the methodical approach, we conducted a comprehensive hindcasting analysis. This exercise allowed us to reconstruct and examine the spatiotemporal evolution of wildfire probability thresholds during the period of 1–15 July 2022, when several wildfire events affected the study area.

5 Results

5.1 Wildfire inventory and modeling sample

In South Tyrol, the initial dataset contained 608 recorded wildfires. After applying the temporal filter, eight events occurring before the year 2000 were excluded, resulting in a final dataset of 600 wildfires. In Trentino, the initial inventories comprised 4,196 wildfires in total. We did not use the first inventory—comprising 1,062 events from the period from 1966 to 1983—due to missing temporal information. From this subset of 3,164 wildfires, we kept only those occurring within our period of interest (2000–2023), leaving 946 wildfire events. Additionally, we filtered out the records without a daily timestamp, resulting in a sample size of 507 wildfires. The two processed inventories were merged, yielding a combined dataset of 1,107 wildfire records. These records met the criteria of having a recorded occurrence date between 2000 and 2023 and an associated daily timestamp. Finally, events with a *burned area* smaller than 50 m^2 were filtered out, resulting in a final dataset of 998 wildfires, which we used in subsequent analysis.

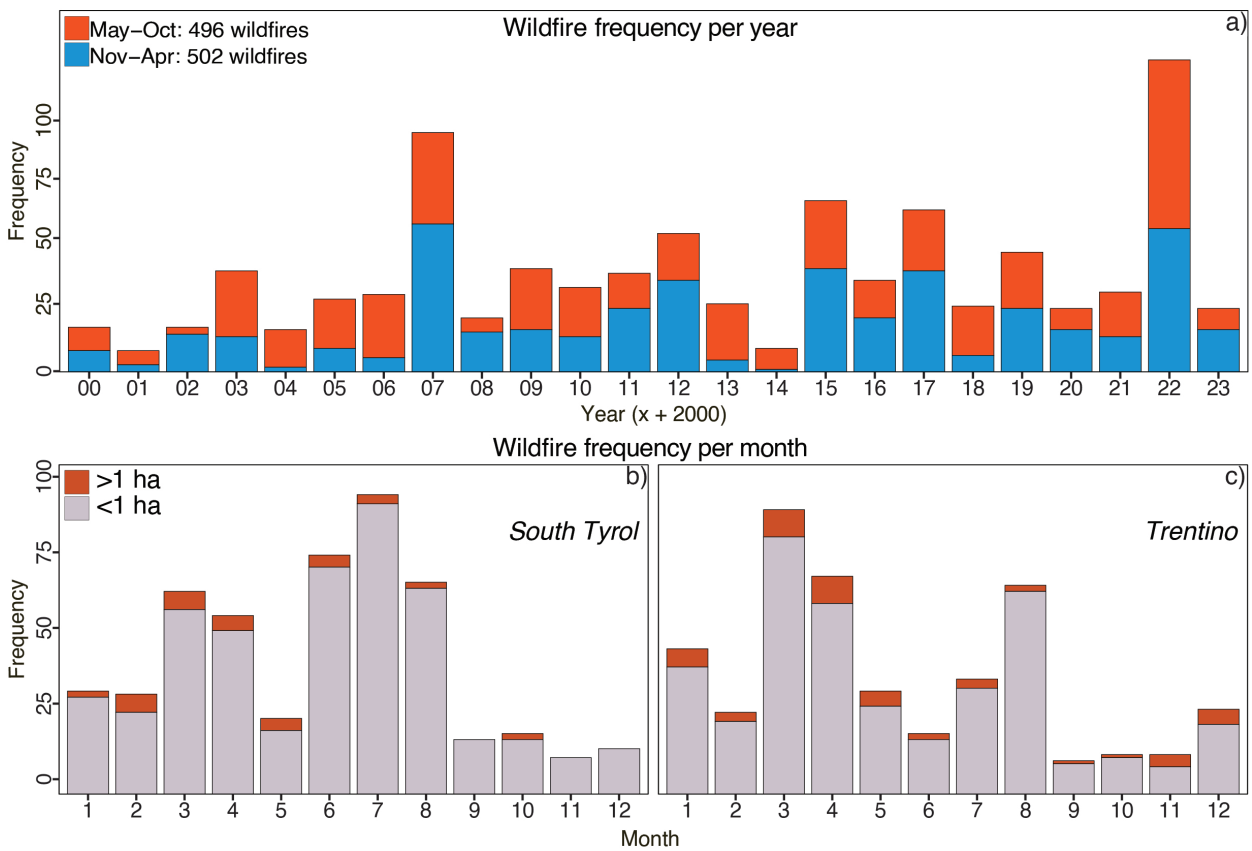

Figure 2: Temporal distribution of wildfires (n = 998) in the study area between 2000 and 2023. Panel (a) shows the annual wildfire counts, distinguishing between events occurring in the warmer months (May—October) and colder months (November—April). Panels (b) and (c) display the monthly distribution of wildfires, with a distinction based on the respective burned area.

Although a detailed characterization of the wildfire regime is not the primary focus of this research, we find it valuable to illustrate some general patterns observed in the inventories. The temporal distribution of wildfires across the study area reveals several notable peaks, as shown in Figure 2a. The most prominent years were 2007 and 2022, each registering over 100 wildfire events each year. Other years with elevated activity—each exceeding 50 wildfires—include 2012, 2015, 2017, and 2019. Monthly trends, in Figures 2b–c, show two seasonal peaks in wildfire occurrence: one in early spring and another in mid-to-late summer. While both South Tyrol and Trentino follow this bimodal pattern, South Tyrol tends to experience more wildfires during the summer peak, whereas Trentino shows a more pronounced peak during the early spring. Regarding weekly patterns, approximately 30% of wildfires occurred during weekends (i.e., Saturday and Sunday), while the remaining 70% took place on weekdays. Between 2000 and 2023, the study area experienced an annual average of 41 wildfires, burning approximately 31 hectares per year. Wildfires occurred throughout the year and were recurrent phenomena both in the warmer months (May–October) and in the colder ones (November–April). Although some years show a clear predominance of wildfires in one period over the other, the overall distribution between warm and cold months remains relatively balanced. In terms of wildfire size, the majority of wildfires were relatively small: 84 out of the 998 events exceeded 1 ha, and only one surpassed 90 ha. Regarding wildfire causes, available only for events in South Tyrol. Roughly 50% of the events have no reported cause. Among the identified causes, lightning accounted for 23%, cigarette-related ignitions for 11%, while the remaining causes included poorly maintained electrical infrastructure, agricultural burns, recreational activities, and arson.

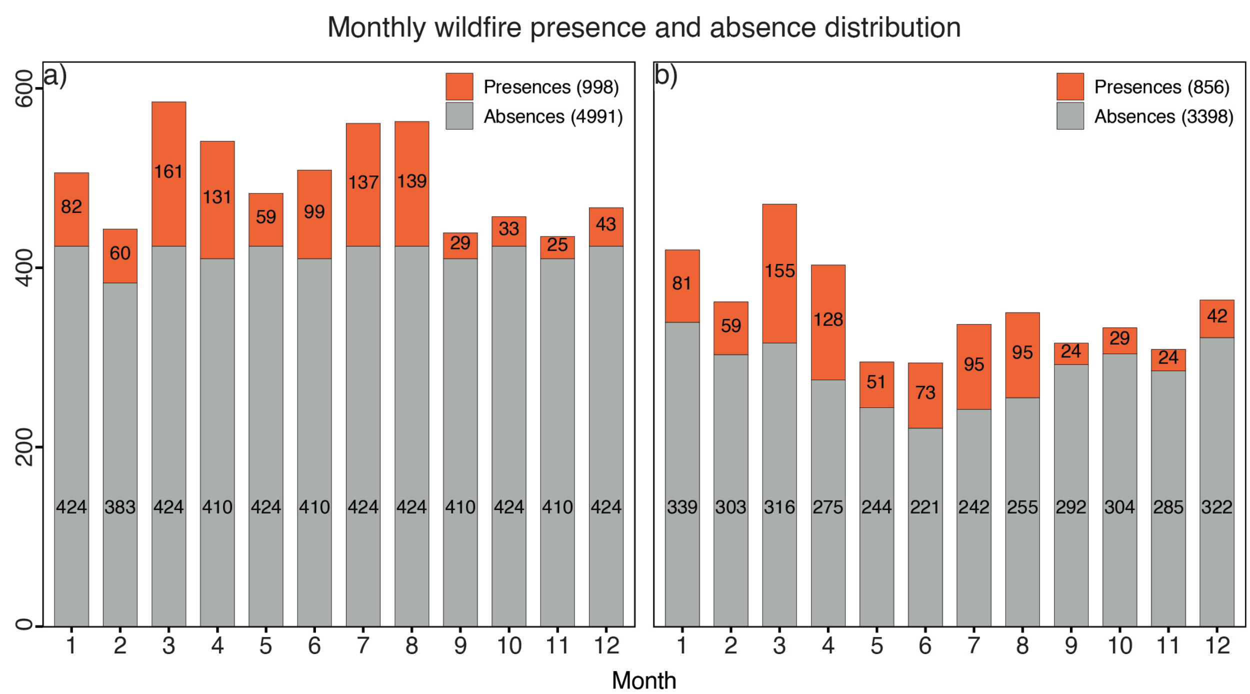

Figure 3: Data sampling results. Bar plots show the monthly distribution of the sample data, wildfire presences (in red) and absence observations (in gray) before (a) and after (b) excluding trivial periods from the dataset.

The final modeling dataset was derived from a combination of wildfire presence and absence samples, totaling 5,989 observations. This included 998 wildfire presences and 4,991 absence observations, respectively, maintaining an approximate 1:5 ratio. To avoid an uneven temporal representation, absence observations were uniformly distributed across years (2000–2023), with proportional representation across months, ensuring that each day of the year had an equal chance of being selected (Figure 3a. At this stage, the sample reflected only the spatial and temporal structure of wildfire presence and absence samples without considering whether the respective observation experienced precipitation. We applied a precipitation-based threshold to account for trivial periods, specifically removing observations with the precipitation on the day of observation (i.e., day 0) equal to or exceeding 1 mm. This filtering step led to excluding 1,735 observations, reducing the sample size to 4,254 records. The impact was more pronounced in the absence data, with nearly 30% of those records excluded, dropping from 4,991 to 3,398. This shows that a significant portion of the absence samples occurred on "dry" periods, with approximately 70% of these experiencing no measurable precipitation (Figure 3b.

Wildfire presence data was also affected, with 142 events——around 15% of the initial wildfire sample——removed. Most of these excluded wildfire records occurred during the summer months (June–August), indicating that a notable number of wildfires were associated with precipitation ≥1 mm on the day of occurrence. This observation underscores the complexity of wildfire-weather interactions during the wetter summer period, where precipitation does not prevent ignition.

5.2 Optimal time windows and modeled relationships

The final modeling dataset was used in a repeated 10-fold RCV with 10 repetitions to identify the optimal time windows for representing the meteorological predictors *P* and *Te* in wildfire prediction (Figure 4).

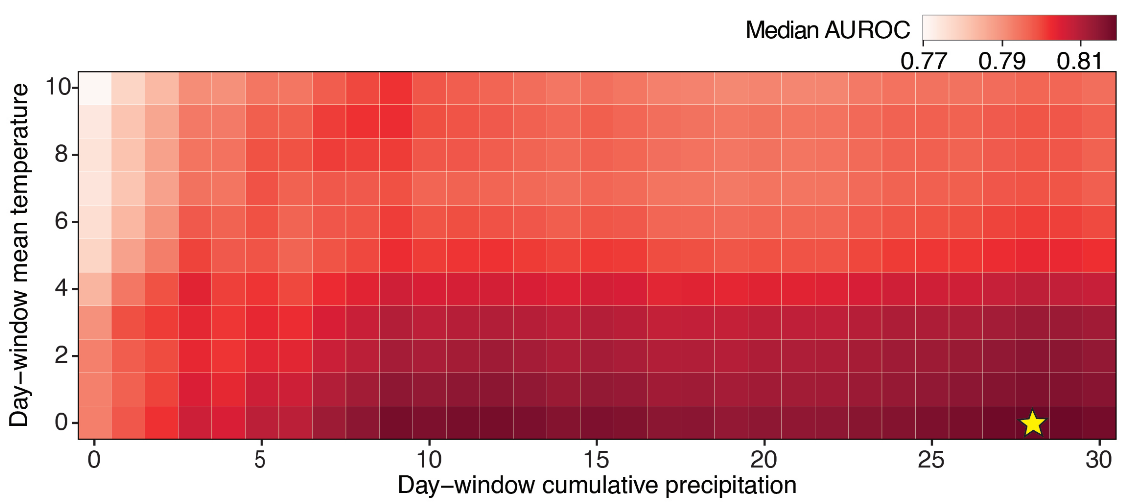

Figure 4: Results of the grid search for optimal *Te*–*P* time window combinations. The plot shows the median AUROC values obtained for each combination of *Te* and *P*, using a 10-fold RCV with ten repetitions. The best-performing combination (yellow star) yielded a mean AUROC of 0.82 and corresponds to the mean temperature on the observation day (Te_0) combined with the cumulative precipitation over the 29 days preceding the event (P_{28}).

Among the tested combinations, the pairing of Te_0 and P_{28} led to the highest model performance, achieving a median AUROC of 0.82. In this configuration, Te_0 denotes the mean daily temperature on the observation date, while P_{28} corresponds to the cumulative precipitation over the preceding 29-day period. Overall, model performance was highest when short temperature windows (e.g., Te_0 to Te_4) were paired with medium precipitation windows (e.g., P_{10} to P_{30}). In contrast, lower AUROCs were observed when longer temperature windows (e.g., Te_5 to Te_{10}) were combined with short or medium precipitation windows (e.g., P_0 to P_{15}). Based on these results, Te_0 and P_{28} were selected as the optimal dynamic predictors and were subsequently integrated with static predictors to develop the final wildfire dynamic model.

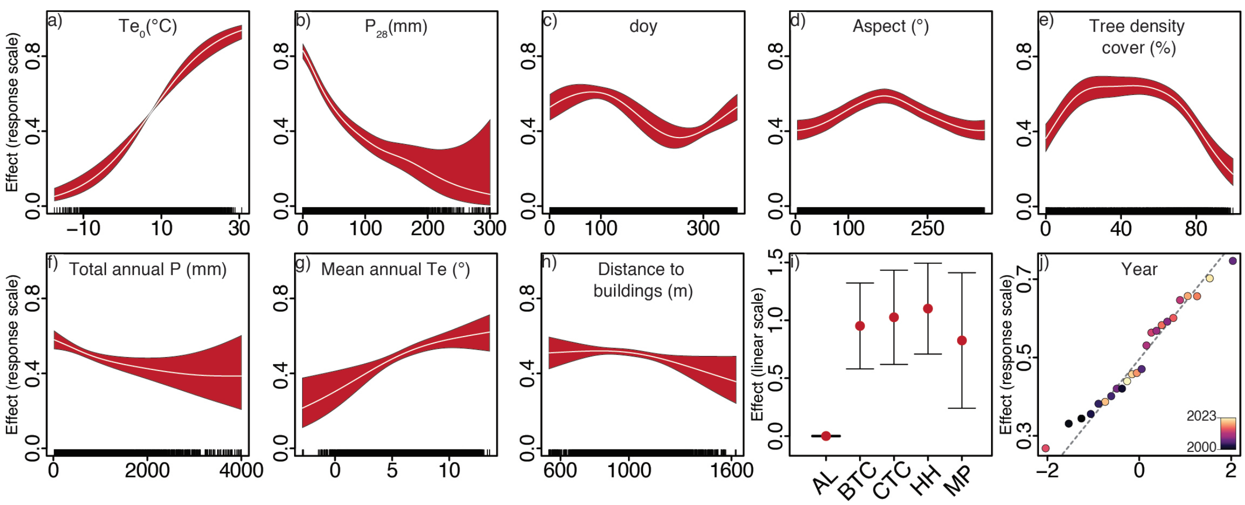

Figure 5: Partial effect plots. Panels (a)–(h) display the partial effects of continuous predictors on the response scale, with the center white lines representing the mean estimated effects, and the red bands indicating the 95% confidence intervals. Panel (i) shows the effect of the categorical predictor *land cover* on the linear scale, where red dots represent the mean estimated effect and error bars indicate the 95% confidence intervals. Lastly, panel (j) illustrates the predictor *year*, which was modeled as a random effect, but excluded during the final prediction phase.

Figure 5 illustrates the partial dependence of selected predictors on wildfire probability, with the influence of all other predictors held constant. The dynamic predictors Te_0 and P_{28} indicated that the highest wildfire probabilities occurred under conditions of elevated Te_0 and limited P_{28}. In contrast, wildfire probabilities were the lowest when P_{28} was abundant and Te_0 was relatively low. The *doy* revealed a seasonal trend, with increased wildfire probabilities around doy_{100}, corresponding to early spring (March–April), and lower probabilities around doy_{250}, which aligns with the late summer (August–September). Among topographic variables, *Aspect* showed a clear pattern: slopes facing south (135°–225°) were associated with a higher likelihood of wildfire occurrence compared to other orientations. In terms of vegetation structure, *tree cover density* revealed that moderate values (20–70%) were linked to increased wildfire probability, whereas sparse (<20%) and dense (>70%) tree cover were linked to reduced probabilities. The *distance to buildings*, used as a proxy for anthropogenic influence, displayed a clear decreasing trend in wildfire probability with increasing distance from built-up areas. The *mean annual temperature*, indicative of generally warmer regions, exhibited a relatively linear relationship, where hotter areas were related to a higher likelihood of wildfire occurrence. Likewise, *total annual precipitation*, serving as a proxy for overall dryness, revealed a relatively linear trend with drier areas being more prone to wildfires. The *land cover*, when using *agricultural land* as the reference category, several classes—including *deciduous tree cover*, *coniferous tree cover*, *herbaceous vegetation and heathland*, and *marshes and peatbogs*—were significantly associated with higher wildfire probability. Finally, *year* was incorporated into the model fit as a random effect to account for the interannual variability in the reported wildfire reporting. Then, it was subsequently excluded from the predictions to ensure that inconsistencies did not systematically influence the resulting wildfire probabilities in the temporal distribution of reported events.

5.3 Variable importance and model evaluation

Permutation variable importance analysis revealed positive contributions from all selected predictors to the model deviance explained. The 29-day accumulated precipitation (P_{28}) emerged as the predominant predictor, followed by temperature at the observation day (Te_0). Among the static environmental factors, *tree cover density* and *land cover* demonstrated relatively high variable importance, while the dynamic *doy* and topographic variable *aspect* exhibited moderate influence. The remaining predictors, while still contributing positively to model deviance explained, displayed comparatively lower relative importance.

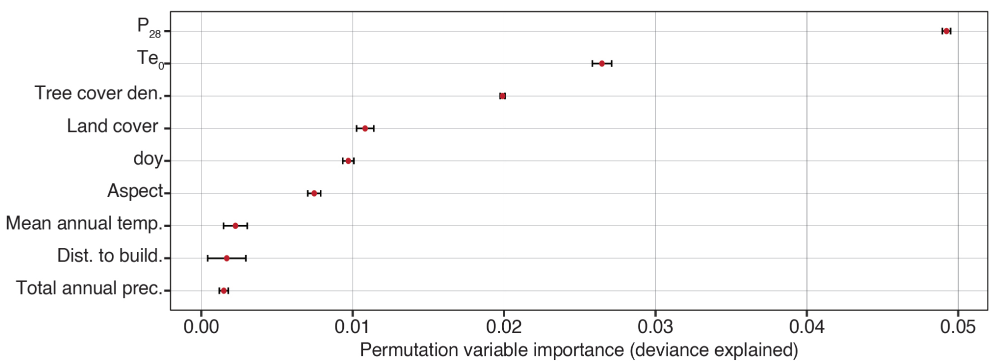

Figure 6: Permutation variable importance results. The red dots denote the mean portion of deviance explained, and the error bars denote the associated standard deviation.

The model exhibited robust predictive capability across all validation routines presented in Figure 7. AUROC scores generally exceeded 0.80, corresponding to *excellent discrimination* as defined by Hosmer et al. (2013). The two 10-fold cross-validation strategies, RCV and SCV, yielded median AUROC values of 0.83 and 0.81, respectively. As anticipated, SCV—which employs k-means clustering to account for spatial autocorrelation—resulted in a slightly lower performance and a broader interquartile range (IQR) than RCV.

The leave-one-out cross-validation routines, namely TCV for years and months, and FCV for land cover, as shown in Figures 7c–d, yielded mean AUROC values of 0.82, 0.79, and 0.79, respectively. The lower performance score across specific folds (years, months, and land cover classes) likely reflects discrepancies between the local conditions driving wildfire occurrence in those subsets and the patterns learned from the remaining data used for the training. TCV at the annual level, in general, demonstrates high temporal transferability, with comparatively lower performance observed in 2002, 2016, and 2018, and higher AUROC values in 2008, 2012, and 2014. On a monthly scale, October exhibits the lowest scores, while the winter months, December–February, yield the highest predictive performance. FCV indicates AUROC values consistently exceeding 0.75 across all land cover classes except for the *agricultural land*, which showed a lower score of approximately 0.72.

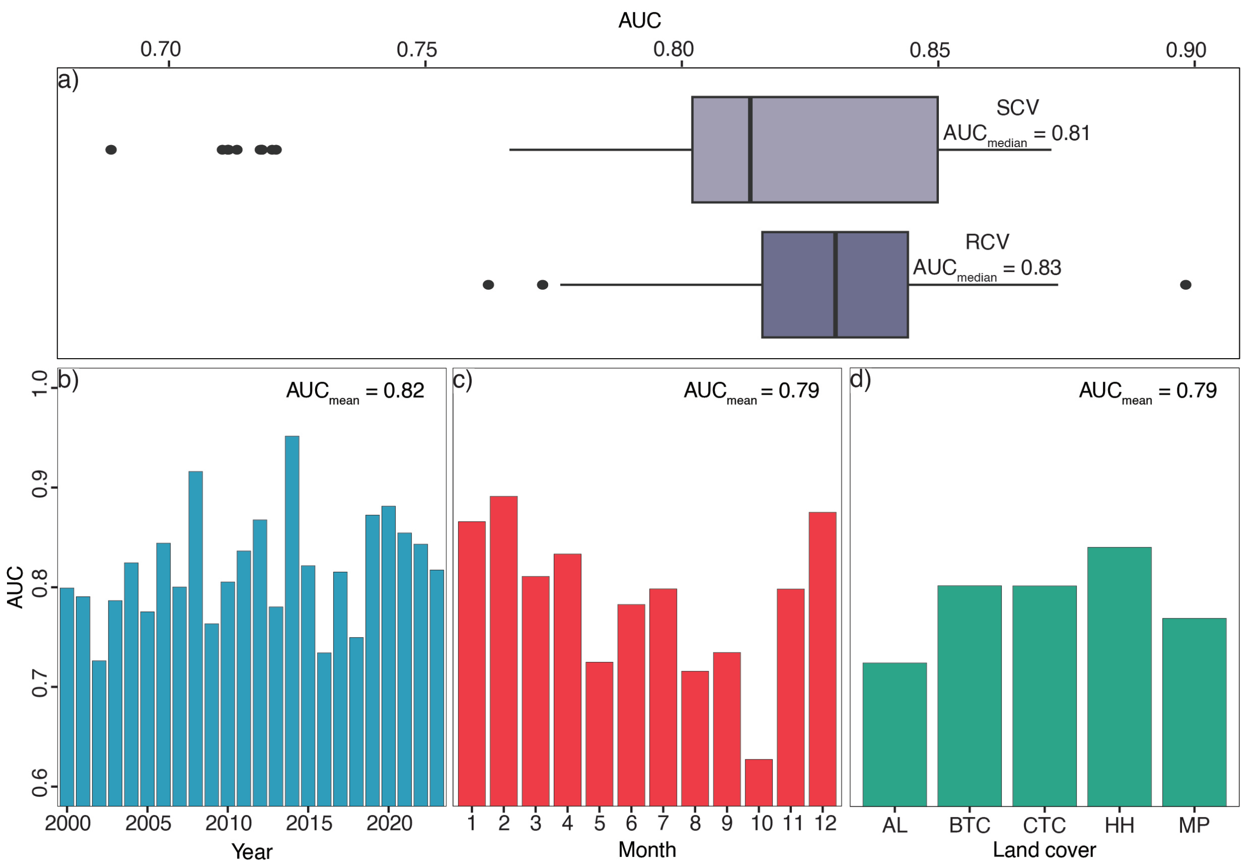

Figure 7: Summary of the predictive model performance. Panel (a) presents the 10-fold RCV and 10-fold SCV results with ten repetitions. Panels (b–c) display the results of the TCV across individual years and months, while panel (d) shows the FCV across different lad cover classes.

5.4 Spatial dynamic thresholds and predictions

The *Te*–*P* heatmap in Figure 8 provides a visualization of the relationship between temperature and precipitation, and their association with wildfire probabilities. In this analysis, static factors and *doy* were excluded from the predictions. The heatmap reveals that the highest wildfire probabilities are predicted under conditions of elevated Te_0 combined with reduced P_{28}. This relationship is highlighted by the spatial distribution of the modeling samples—with their respective Te_0 and P_{28} values—within the heatmap. Wildfire occurrences (denoted by crosses) are predominantly clustered in regions of higher probability, while absence observations (denoted by points) concentrate in areas with lower probability scores.

The selected thresholds act as decision boundaries distinguishing between areas with high and low predicted wildfire probabilities. In other words, predictions below a given threshold indicate low wildfire probability, while those above suggest high wildfire probability scores. For instance, 95% of the wildfire occurrences exceed the *TPR95* (green dotted line) threshold, but a low proportion of correctly classified absences (TNR of 41%) fall below this threshold, implying relatively high false alarms (FPR of 59%). Conversely, the more conservative *TPR35* (blue dotted line) threshold minimizes false alarms (FPR of 5%) by correctly classifying 95% of absences (TNR of 95%), but identifies only 35% of wildfire occurrences. The *OPT* threshold (red solid line) provides a balanced trade-off, achieving a TPR of 77% while maintaining an FPR of 25% (TNR of 75%). To put it in another way, this threshold optimizes the identification of wildfire occurrences while keeping an acceptable level of correct absence classification.

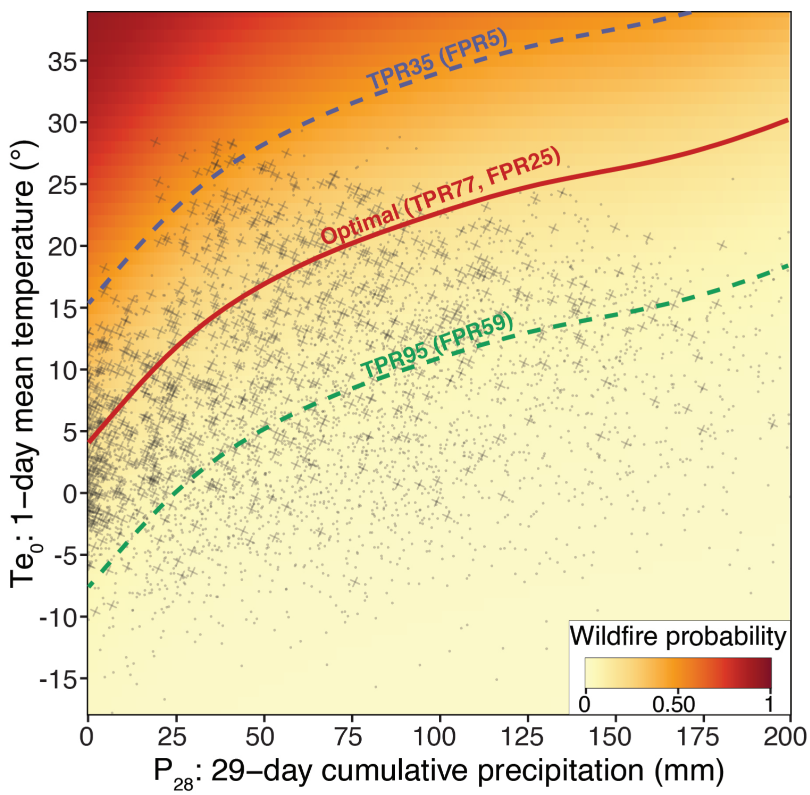

Figure 8: *Te–P* heatmap showing the predicted wildfire probability in relation to temperature and precipitation inputs. The plot illustrates the combined effect of *Te* and *P* on the predicted probability of wildfire occurrence, assuming average values for *doy* and all static predictors (i.e., *aspect*, *tree cover density*, *total annual precipitation*, *mean annual temperature*, *distance to buildings*, and *land cover*). Crosses represent the 859 wildfires, while points indicate the 3,398 absence observations. The curves correspond to the selected probability thresholds: *TPR95* (green), *OPT* (red) and *TPR35* (blue).

The heatmap and thresholds highlight the relationship between dynamic predictors, prediction scores, and the link to the ROC curve. Furthermore, the probability thresholds demonstrate a potential application of our model for early warning systems, analogous to established landslide probability thresholds, and provide flexibility in implementation based on specific wildfire management objectives. It is important to note, however, that accurate visualization of these heatmaps also requires the integration of static factors.

Figure 9 illustrates how seasonal variations and changes in static environmental conditions influence the *Te*–*P* relationship with wildfire probability. Specifically, we performed a comparative analysis of the *Te*–*P* heatmaps across different combinations of *doy*, *aspect*, and *tree density cover*, with the remaining predictors being excluded.

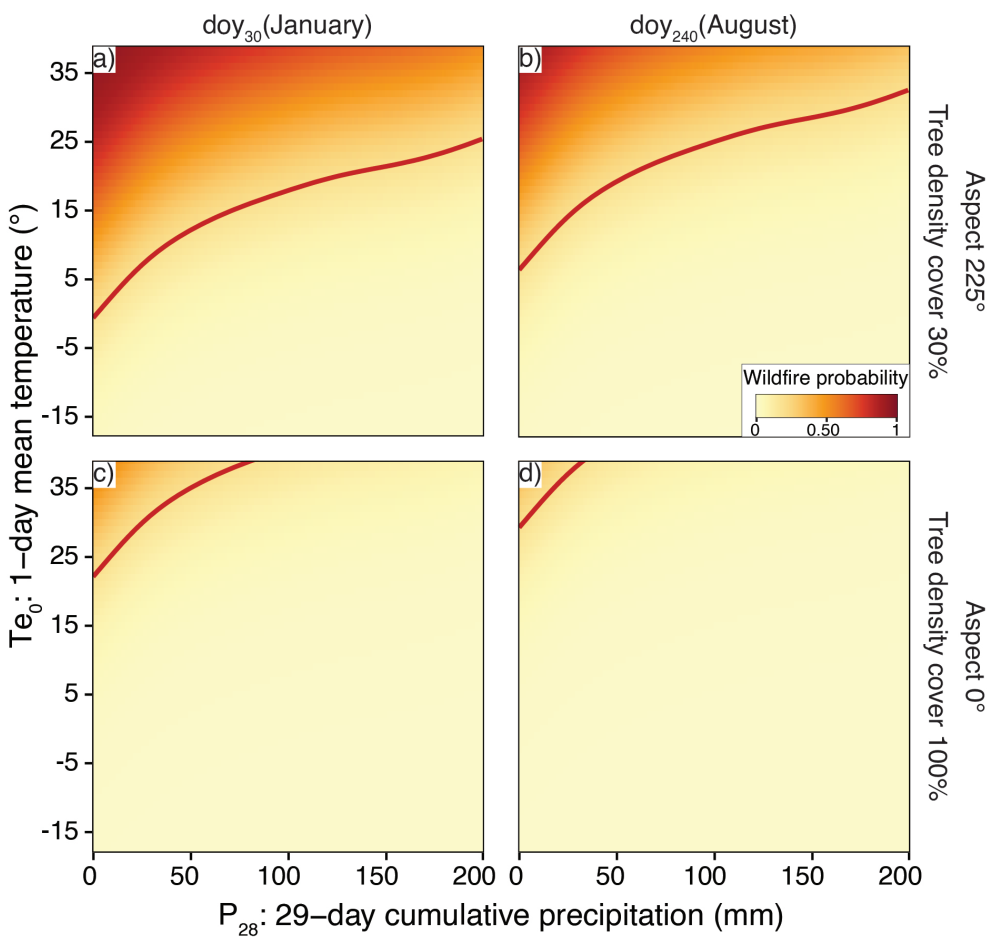

Figure 9: *Te*–*P* heatmaps showing the predicted wildfire probability for increasing amounts of *Te* and *P* and associated *OPT* threshold for different combinations of *doy* (doy_{30} and doy_{240}), *aspect* (225° and 0°) and *tree density cover* (30% and 100%).

Panels (a, c) versus panels (b, d) demonstrate the influence of the seasonal variation through *doy*. It is observed that substantially lower short-term temperature Te_0 is required to exceed the *OPT* wildfire probability threshold on a winter day (doy_{30}) compared to a summer day (doy_{240}), where higher amounts of Te_0 are necessary to reach equivalent predicted probabilities. By contrasting Figure 9a–b versus Figure 9c–d, we investigate the role of topographic orientation and vegetation structure. The former set of panels represents conditions with a south-facing *aspect* of 225° and a relatively low *tree cover density* of 30%, whereas the latter reflects a north-facing *aspect* of 0° and dense forest cover (100%). The heatmaps reveal that substantially higher Te_0 and lower P_{28} are necessary to achieve high wildfire probabilities and exceed the *OPT* threshold under conditions of dense vegetation and in north-facing slopes. Such analyses can be extended to any combination of predictors in the model and offer valuable insights into the spatiotemporal dynamics of wildfire occurrence.

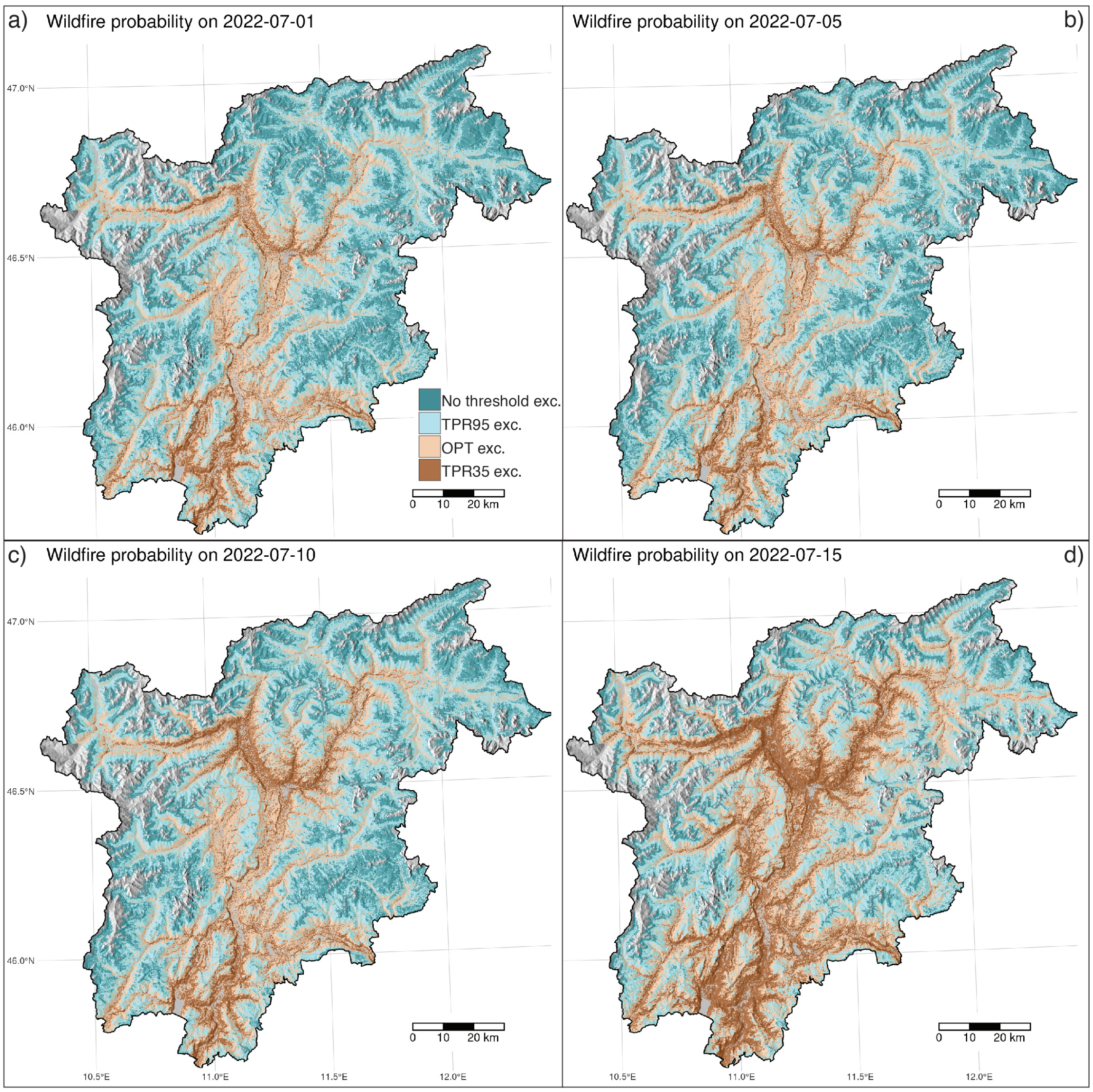

Figure 10: Hindcasting example of wildfire occurrence during the period between 1–15 July 2022. The illustrations display the spatial distribution of the predicted wildfire probability across the entire study area using the three selected probability thresholds: *TPR95*, *OPT*, and *TPR35*.

To further demonstrate the model potential applications, we conducted a hindcast analysis covering the period of 1–15 July 2022—a timeframe chracterzied by elevated wildfire activity across the study region. The resulting model predictions, initially expressed as continuous probabilities, were subsequently reclassified using the predefined thresholds

(*TPR95*, *OPT*, and *TPR35*). Figure 10 presents four representative snapshots at 5-day intervals from this period, illustrating the temporal evolution of predicted wildfire probability thresholds. These sequential images reveal a pronounced increase in predicted wildfire occurrence as the date approaches mid-July, with substantial expansion of areas exceeding the *OPT* and *TPR35* thresholds. The spatial patterns emerging from these predictions show notable regional variability, with specific zones—particularly the inner valley bottoms—consistently exceeding both the mid and high probability thresholds throughout the analysis period. This spatial heterogeneity reflects differences in the underlying environmental characteristics across the landscape, including topography, infrastructure, vegetation, land cover, and meteorological conditions. A pronounced transition is observed between 10 and 15 July, during which several inner-valley areas surpass the highest threshold, indicating high probability scores. The complete temporal overview of the hindcast is available as an animated GIF (*Trentino–SouthTyrol.GIF*), offering a dynamic visualization of how predicted wildfire probability thresholds evolved throughout this two-week window.

6 Discussion

In this study, we implemented an interpretable spatiotemporal modeling framework that integrates static environmental and dynamic meteorological factors to predict wildfire occurrence. The model demonstrates strong predictive capabilities, with AUROC values generally exceeding 0.80, highlighting its effectiveness in capturing key drivers of wildfire initiation. These included static landscape features, daily temperature and precipitation fields, and a seasonal proxy. The following discussion addresses critical aspects of the study, including reflections on model interpretability and flexibility, considerations related to wildfire processes and drivers, and the applicability of the model in early warning.

6.1 Model flexibility and interpretability

The sampling strategy played a key role in constructing the modeling dataset. As the quality and representativeness of the input data heavily influenced the model outcomes, careful design of the sampling process is as relevant as the modeling phase itself. While many data-driven studies emphasize comparing algorithms, evaluating data preparation and sampling strategies is often underappreciated. Generating the modeling sample involves filtering the wildfire presences and sampling the absence observations due to the large disproportion between the two. The selection of wildfire presences—conditioned on the availability of historical records—enables event filtering based on the attributes in the wildfire inventory, e.g., *date of occurrence*, and *burned area*. In contrast, sampling absence observations, especially in the spatiotemporal domain, offers broader flexibility. In this research, the absence sampling was guided by set of structured rules: as detailed in Section 4.1, we (a) masked out trivial terrain based on land cover data, (b) implemented temporal buffers in locations that experienced wildfires before, (c) ensured temporal balance by sampling across different years and months, and (d) excluded trivial periods. These steps collectively aimed to reduce sampling biases and improve the model generalization.

The modeling approach considers the integration of static and dynamic factors to account for the complex interplay of wildfire occurrence. An advantage of this framework is the interpretability of the model outcomes, which we briefly highlight in the following discussion. The optimal time window analysis identified that the combination yielding the highest predictive performance includes Te_0, the mean daily temperature on the observation day, and P_{28}, the cumulative precipitation over the preceding 29 days (see Figure 4). While this combination achieved the highest median AUROC, it is noteworthy that performance differences among alternative time window configurations were relatively small, with AUROC values ranging from 0.77 to above 0.81. This reinforces the importance of precipitation and temperature as dynamic predictors, while also indicating that the model results are relatively stable and not highly sensitive to changes in the selected time windows.

Regarding the modeled relationships illustrated in Figure 5 *Aspect* depicts high probabilities in slopes facing south (135°–225°). In the northern hemisphere, south-facing slopes receive more solar radiation during the day than others, and this translates to lower average moisture levels and thus increasing wildfire probabilities, as several studies indicate (Alexander et al., 2006; Oliveira et al., 2013; Oliveras et al., 2009). The *tree density cover* reveals that areas with very sparse tree cover (<20%), may lack sufficient fuel to sustain wildfires, while densely forested areas (>70%) appear to be more resilient to wildfire initiation due to forest microclimate effects—tendency to be cooler, more humid and with less sun exposure. In contrast, regions with intermediate and fragmented tree density cover (20–70%) exhibit the highest wildfire probabilities, likely due to a combination of fuel availability and increased edge effects (Song et al., 2017; Rotbarth et al., 2025).

The *total annual precipitation* was used as a proxy to represent the spatial variability of long-term precipitation regimes across the study area. The results indicate that drier regions are more susceptible to wildfire occurrence, whereas wetter areas are associated with lower wildfire probabilities. Similarly, the *mean annual temperature* captures broader spatial thermal gradients, revealing that relatively warmer zones are generally more prone to wildfires than colder ones. These drier and warmer areas tend to exceed the critical probability thresholds earlier under specific temperature and precipitation conditions, compared to their wetter and cooler counterparts.

Although the wildfire inventory lacks the specific data on the fire causes for our study area, previous research in comparable alpine regions has identified human activity as a dominant ignition source (Arpaci et al., 2014; Müller et al., 2020b; Arndt et al., 2013; Müller et al., 2020a). In our analysis, *distance to buildings* was used as a proxy to account for anthropogenic influence. The results indicate that areas closer to infrastructure—and thus more accessible to human activity—are associated with higher wildfire probability. Initially, *distance to roads* was also considered an additional proxy; however, including both predictors in the model fit introduced redundancy, leading to the loss of statistical significance in one of them. Therefore, we retained only *distance to buildings*, given its broader spatial representation of human influence.

The *land cover*, identified as the second most influential predictor, served as a proxy for fuel availability. Compared to the reference category *agricultural land*, all other classes exhibited association with higher wildfire probability. Overall, *agricultural land* appeared to be the least prone to wildfire occurrence. Among the remaining classes, *marshes and peat-bogs* were slightly less preferred regarding wildfire occurrence. Both *coniferous tree cover* and *broadleaf tree cover* showed nearly identical regression coefficients, suggesting a comparable influence on wildfire probability—consistent with the findings reported in Müller et al. (2020a). The *herbaceous vegetation and heathland* class displayed a slightly higher coefficient, pointing to increased fire likelihood. This supports the conclusions in Oliveira et al. (2013), where it was reported that shrublands, grasslands, and sparsely vegetated areas are more prone to ignition due to their intrinsic flammability and ease of combustion.

The predictor *doy*, used as a proxy for seasonal effects, is expected to capture the temporal distribution of wildfire occurrences throughout the year. However, since the model already incorporates two dynamic predictors, P_{28} and Te_0, which inherently exhibit seasonal variability, we interpret the effect of *doy* as capturing residual seasonality not explained by these two meteorological predictors. Notably, the model reveals elevated wildfire probability in early spring, a period typically associated with rapid warming and snowmelt. This suggests that the selected meteorological predictors may be less effective in fully capturing the seasonal dynamics influencing fire occurrence during this transitional period. Conversely, *doy* indicates comparatively lower fire probabilities during summer, which we interpret as evidence that P_{28} and Te_0 already account for much of the seasonal variation during that time. In practical terms, this implies that the wildfire probability may be higher in early spring than in late summer for a given location and under the same precipitation and temperature conditions.

These results are a sample of the complex interplay between dynamic meteorological and static environmental factors in determining wildfire probability, providing quantitative insights into the spatiotemporal dynamics of wildfire occurrence across the landscape. Also, the analysis shows that identical meteorological conditions can produce markedly different wildfire probabilities depending on the underlying environmental context, highlighting the importance of incorporating dynamic and static predictors in wildfire assessment.

6.2 Limitations and future perspectives

Among all the predictors, the 29-day cumulative precipitation P_{28} and the 1-day mean temperature Te_0 emerged as the most influential ones in the model, as shown in Figure 6. Both P_{28} and Te_0 act as proxies for fuel moisture, so that drier fuels, resulting from prolonged dry and warm periods, are more prone to wildfire ignition than moist fuels. Hence, lower cumulative precipitation and high temperature levels reflect higher wildfire occurrence probabilities. However, limitations arise from the use of these two predictors. The use of absolute values in precipitation and temperature may mislead the results, since equal levels of these two meteorological predictors can have different impacts depending on the local climatologies. For instance, an area experiencing usually high temperatures and anomalously low precipitation—relative to the long-term averages—may exhibit heightened wildfire probabilities compared to an area with equal static settings for which such dynamic conditions are typical. In our model, we included *total annual precipitation* and *mean annual temperature* averaged over 30 years to partly account for these climatologies.

Still, the variable importance assessment indicated they were among the least influential predictors. We believe that the use of anomalies in the precipitation and temperature, rather than absolute values, could provide the means to directly account for the climatologies and improve the overall interpretability of the model. Future perspectives of the model could benefit from integrating indices such as temperature anomalies (e.g., daily deviations from the climatological means) or counts of days above-below specific temperature thresholds. In terms of precipitation widely recognized drought indicators such as the standardized precipitation index (SPI; McKee et al., 1993) or the standardized precipitation evapotranspiration index (SPEI; Vicente-Serrano et al., 2010) could be implemented. These indices offer standardized, temporally dynamic representations of hydrological stress and have proven valuable in capturing preconditions favorable for wildfire occurrence (Turco et al., 2017, 2018; Smith et al., 2023).

In a similar context, one of the most relevant, yet underrepresented aspects in this model is the role of compound events, particularly droughts and heatwaves. Compound—simultaneous occurrence—hot and dry extreme events can trigger and exacerbate cascading processes such as wildfires (Richardson et al., 2022). Atmospheric heatwaves, defined as prolonged and consecutive periods of anomalously high temperatures, have been consistently linked to increased wildfire activity (Barriopedro et al., 2023). Similarly, "hot drought" conditions (characterized by warm temperatures and simultaneous meteorological drought) represent elevated fire-weather types. Recent studies have identified two heat-induced fire-weather types, "heatwave" and "hot drought", which collectively account for nearly 50% of wildfires in the Mediterranean region (Ruffault et al., 2020; Santos et al., 2024). These events are marked by significantly elevated temperatures, low humidity, and dry fuels, often with anomalous values compared to surrounding days. Including compound drought and heatwave indices in such a model would allow a more realistic characterization of wildfire scenarios (Lemus-Canovas et al., 2025), especially in light of expected increases in their frequency under global warming (Felsche et al., 2024).

As is the case for the meteorological predictors, further model improvements could involve expanding some static predictors into dynamic representations. For example, *land cover*, used as a proxy for fuel type, could be replaced or complemented by dynamic fuel maps that reflect seasonal changes in vegetation structure and flammability. Similarly, the anthropogenic influence—currently represented by static proximity to infrastructure—could be much further elaborated through time-varying proxies such as mobility data, population fluxes, or seasonal tourism patterns (Pittore et al., 2023; Renner et al., 2018). Another limitation pertains to uncertainty in the wildfire inventory. In South Tyrol, the dataset is point-based, yet the meaning of these points, whether they represent ignition locations or random points within burned polygons, is unclear. In Trentino, wildfire points were generated from polygon centroids, assuming that ignition occurs at the spatial center of the fire. This spatial uncertainty could affect the accuracy of predictor extraction, particularly for sensitive predictors. Furthermore, another point of improvement could be adding the potential wildfire spread in addition to the occurrence probability. Incorporating fire spread in a second-stage model would require a potentially different modeling framework and additional predictors (e.g., wind speed and direction, slope steepness; Povak et al., 2018; Linn et al., 2007; Jellouli et al., 2022). Such an extension could significantly enhance the predictive utility of the framework, particularly for operational or early-warning applications.

To better tailor the model toward dry conditions, we applied a threshold-based filtering to exclude periods characterized by excessive precipitation. However, the downside of this approach is that it removed a significant number of summer wildfire records, many likely linked to convective storms and lightning activity. These events are particularly important in alpine regions, where afternoon thunderstorms are frequent and lightning is a known natural ignition source. As a result, our model may underrepresent lightning-induced fires, specifically those occurring during so-called "wet" periods. In future developments, we recommend including classified atmospheric circulation patterns (Lemus-Canovas et al., 2019) as part of the filtering rule to better account for lightning-induced events.

Wildfires are more complex than other natural hazards, which often have natural physical triggers. A wildfire can only occur if a source of ignition is present, such as lightning as a natural source, or the much more frequent (in)direct human influence (Chuvieco et al., 2003; Müller et al., 2020a). While our model includes a proxy for anthropogenic influence, *distance to buildings*, it does not explicitly account for lightning or human influence as triggers. As such, the model outputs should not be interpreted as a pure relative probability of wildfire initiation, but rather as the probability of an area experiencing a wildfire given that ignition occurs (human or lightning). This distinction is crucial, particularly when using the model to inform practitioners. In this context, the spatial predictions reflect the relative predisposition of the landscape to wildfires under specific static terrain and dynamic meteorological conditions. Future studies should explore more direct proxies of human activity, such as forest trail density, proximity to power lines, proximity to cable cars, mobility datasets, and investigate multi-scale dynamic factors influencing ignition potential (Arpaci et al., 2014; Chuvieco et al., 2010).

6.3 Considerations on early warning

The most relevant model outcome, the wildfire prediction scores, can be illustrated as continuous probability surfaces (e.g., ranging from 0 to 1) or discrete categorized classes. While the continuous outputs retain the full granularity of the model, categorized maps are often preferred in decision-making contexts for their intuitive representation of different danger levels. However, deriving classes from statistical properties of the data distribution, such as quantiles, geometry, and standard deviation, can obscure the practical meaning and limit the interpretation for end-users. To address this, we adopted the classification strategy proposed in Steger et al. (2023), which categorizes raw probabilities based on their association with key performance metrics such as the TPR and false alarms, which hold particular relevance in early warning. Among the evaluated thresholds, the optimal cut-off *OPT* provided a balanced trade-off, capturing 77% of observed wildfires while limiting the false alarms to 25%. Alternative threshold such as the *TPR95* (high sensitivity) and the *TPR35* (low false alarms) allow the approach to be tailored to different risk priorities. Such priorities can be seen in a context where a false alarm may lead to unnecessary allocation of resources, whereas a missed alarm may have more severe consequences—–such as failing to issue timely warnings and inadequate preparedness for wildfire events. However, as our results show, prioritizing high sensitivity (95%) substantially increases false alarms (59%), whereas minimizing false alarms (e.g., 5%) comes at the cost of reduced wildfire classification rates (TPR = 35%).

Other approaches for threshold selection are particularly valuable when dealing with imbalanced datasets—such as those with few wildfire observations and many absences—where standard metrics like accuracy may become less informative (Saito et al., 2015). In such contexts, the thresholding can be guided based on the precision–recall curve, where the thresholds are chosen based on the recall (TPR, proportion of actual wildfires correctly classified) and precision (the proportion of predicted wildfire locations that correspond to actual wildfires). This can provide a more meaningful assessment of predictive performance, especially for early warning applications targeting rare but high-impact hazards like wildfires (Patton et al., 2023). In any case, the threshold selection should always be done accordingly to the end-user needs, whether the concern may be the cost of the false alarms or if the tolerance is low to accept almost any alarm.

The temporal analysis showcased in this study confirms the model capacity to reflect dynamic changes in wildfire probabilities in response to evolving meteorological conditions. While originally applied for hindcasting, the model can be extended to nowcasting and forecasting applications, provided that the input levels for precipitation and temperature do not substantially deviate from the fitting dataset. Notably, the model also enables exploratory what-if scenarios, a valuable asset in the context of climate risk preparedness and adaptation planning. For example, users can assess the implications of a drop in cumulative precipitation P_{28} under anomalously high temperatures Te_0 for given static settings and a given seasonal context. Additional scenario-building can explore the role of fuel-related predictors such as changes in *tree cover density* or transitions between *land cover* classes, to evaluate their influence on wildfire probability. This narrative-driven simulations offer a flexible tool to assess potential wildfire outcomes under hypothetical future climatic conditions and support more informed and forward-looking decision-making in wildfire risk management.

Our model delivers wildfire predictions at a relatively high spatial resolution (50 m) and daily temporal resolution, offering significantly finer granularity than existing global and European early warning systems, such as EFFIS (current resolution: 9 km; Di Giuseppe et al., 2025) and the former global early warning system for wildland fire (https://gfmc.online/gwfews/index-12.html; de Groot et al., 2006), suspended on 2021. This high-resolution capability is particularly advantageous in complex Alpine environments like our study area, where wildfires tend to be small-scale and spatially heterogeneous. Nevertheless, benchmarking to better understand potential benefits and limitations in model outcomes is still relevant for future perspectives.

7 Conclusion

In this research, we employed GAMs to predict wildfire initiation in space and time, accounting for static terrain attributes and dynamic meteorological conditions in the region of Trentino–South Tyrol, Italy. We captured the meteorological drivers of wildfire occurrence based on a combination of 29-day cumulative precipitation (P_{28}), 1-day mean temperature (Te_0), and day of the year (doy) factor. These dynamic predictors were complemented by static proxies representing fuel type and structure, meteorological predisposition, topographic features, and anthropogenic influence. Particular emphasis was placed on implementing a representative sampling scheme and generating interpretable outputs, including the visualization of the modeled relationships and variable importance. Model predictions were further linked and classified using combinations of true positive rates and false alarms to derive thresholds that support practical applications in the realm of early warning. The model showed strong predictive performance, with AUROC values generally exceeding 0.80 under a rigorous multi-validation framework accounting for spatial and temporal variability. Beyond predictive skill, we illustrated the model utility by hindcasting a two-week period of elevated wildfire activity in July 2022. The flexible framework can be adapted to other natural hazards governed by the interplay of static and dynamic factors. We see our approach as a contribution to the broader development of data-driven solutions that characterize the occurrence of natural hazards through the joint assessment of static controls and time-varying triggers. Crucially, we emphasize that such models should prioritize input data quality, carefully designed sampling strategies, and the interpretability of results to ensure their value in scientific and operational decision-making contexts.

8 CRediT authorship contribution statement

Mateo Moreno: Writing – original draft, Visualization, Validation, Methodology, Formal analysis, Data curation, Conceptualization. **Stefan Steger:** Writing – review & editing, Supervision. **Laura Bozzoli:** Data curation, Writing – review & editing. **Stefano Terzi:** Writing – review & editing. **Andrea Trucchia:** Writing – review & editing. **Cees van Westen:** Writing – review & editing, Supervision. **Luigi Lombardo:** Writing – review & editing, Supervision.

9 Financial support

This research has been supported by the EO4MULTIHA project (4000141754/23/I-DT), funded by the European Space Agency.

10 Code and data availability

The modeling procedure was conducted in R. The scripts are available at the repository https://github.com/mmorenoz/Wildfire_EarlyWarning. The daily precipitation and temperature fields are available in Crespi et al. (2020).

11 Acknowledgement

The research that led to these results is related to the EO4MULTIHA project (https://eo4society.esa.int/projects/eo4multihazards/, which received funding from the European Space Agency (ESA). We thank the Faculty of Geo-information Science and Earth Observation (ITC) – University of Twente for covering the open-access publication fees. We thank Dr. Serkan Girgin for his support in using the CRIB platform. We thank Dr. Paolo Fiorucci and Dr. Marj Tonini for their valuable feedback. Finally, we thank the Office for Forest Planning of the Autonomous Province of Bolzano, especially Alessandro Andriolo, for providing and revising the wildfire data.

References

Adler, S., Chimani, B., Drechsel, S., Haslinger, K., Hiebl, J., Meyer, V., Resch, G., Rudolph, J., Vergeiner, J., Zingerle, C., Marigo, G., Fischer, A. and Seiser, B. (2015) Das Klima: Von Tirol-Sudtirol-Belluno. Report, ZAMG, Autonome Provinz Bozen, ARPAV.

Ager, A. A., Vaillant, N. M. and Finney, M. A. (2010) A comparison of landscape fuel treatment strategies to mitigate wildland fire risk in the urban interface and preserve old forest structure. Forest Ecology and Management **259**(8), 1556–1570.

Alexander, J. D., Seavy, N. E., Ralph, C. J. and Hogoboom, B. (2006) Vegetation and topographical correlates of fire severity from two fires in the Klamath-Siskiyou region of Oregon and California. International Journal of Wildland Fire **15**(2), 237–245. Publisher: CSIRO PUBLISHING.

Alvioli, M., Loche, M., Jacobs, L., Grohmann, C. H., Abraham, M. T., Gupta, K., Satyam, N., Scaringi, G., Bornaetxea, T., Rossi, M., Marchesini, I., Lombardo, L., Moreno, M., Steger, S., Camera, C. A. S., Bajni, G., Samodra, G., Wahyudi, E. E., Susyanto, N., Sinčić, M., Gazibara, S. B., Sirbu, F., Torizin, J., Schüßler, N., Mirus, B. B., Woodard, J. B., Aguilera, H. and Rivera-Rivera, J. (2024) A benchmark dataset and workflow for landslide susceptibility zonation. Earth-Science Reviews **258**, 104927.

Arndt, N., Vacik, H., Koch, V., Arpaci, A. and Gossow, H. (2013) Modeling human-caused forest fire ignition for assessing forest fire danger in Austria. iForest - Biogeosciences and Forestry **6**(6), 315. Publisher: SISEF - Italian Society of Silviculture and Forest Ecology Section: Forest Dynamics and Natural Disturbances.

Arpaci, A., Eastaugh, C. S. and Vacik, H. (2013) Selecting the best performing fire weather indices for Austrian ecoregions. Theoretical and Applied Climatology **114**(3), 393–406.

Arpaci, A., Malowerschnig, B., Sass, O. and Vacik, H. (2014) Using multi variate data mining techniques for estimating fire susceptibility of Tyrolean forests. Applied Geography **53**, 258–270.

Barriopedro, D., García-Herrera, R., Ordóñez, C., Miralles, D. G. and Salcedo-Sanz, S. (2023) Heat Waves: Physical Understanding and Scientific Challenges. Reviews of Geophysics **61**(2), e2022RG000780. _eprint: https://onlinelibrary.wiley.com/doi/pdf/10.1029/2022RG000780.

Bergonse, R., Oliveira, S., Gonçalves, A., Nunes, S., DaCamara, C. and Zêzere, J. L. (2021) Predicting burnt areas during the summer season in Portugal by combining wildfire susceptibility and spring meteorological conditions. Geomatics, Natural Hazards and Risk **12**(1), 1039–1057. Publisher: Taylor & Francis _eprint: https://doi.org/10.1080/19475705.2021.1909664.

Bessie, W. C. and Johnson, E. A. (1995) The Relative Importance of Fuels and Weather on Fire Behavior in Subalpine Forests. Ecology **76**(3), 747–762. _eprint: https://onlinelibrary.wiley.com/doi/pdf/10.2307/1939341.

Bjånes, A., De La Fuente, R. and Mena, P. (2021) A deep learning ensemble model for wildfire susceptibility mapping. Ecological Informatics **65**, 101397.

Bolker, B. M., Brooks, M. E., Clark, C. J., Geange, S. W., Poulsen, J. R., Stevens, M. H. H. and White, J. S. S. (2009) Generalized linear mixed models: a practical guide for ecology and evolution. Trends in Ecology & Evolution **24**(3), 127–135. Publisher: Elsevier Current Trends.

Bovio, G., Quaglino, A. and Nosenzo, A. (1984) Individuazione di un indice di previsione per il pericolo di incendi boschivi. MONTI E BOSCHI Accepted: 2015-05-12T10:13:32Z.

Bowd, E. J., McBurney, L. and Lindenmayer, D. B. (2021) Temporal patterns of vegetation recovery after wildfire in two obligate seeder ash forests. Forest Ecology and Management **496**, 119409.

Brabb, E. E. (1984) Innovative approaches to landslide hazard and risk mapping. In Proceedings of IVth International Conference and Field Workshop in Landslides, volume 1, pp. 307–324. Toronto, Canada: .

Brenning, A. (2012) Spatial cross-validation and bootstrap for the assessment of prediction rules in remote sensing: The R package sperrorest. In 2012 IEEE international geoscience and remote sensing symposium, pp. 5372–5375. IEEE.

Brunetti, M. T., Peruccacci, S., Rossi, M., Luciani, S., Valigi, D. and Guzzetti, F. (2010) Rainfall thresholds for the possible occurrence of landslides in Italy. Natural Hazards and Earth System Sciences **10**(3), 447–458. Publisher: Copernicus Publications Göttingen, Germany.

Cao, X., Cui, X., Yue, M., Chen, J., Tanikawa, H. and Ye, Y. (2013) Evaluation of wildfire propagation susceptibility in grasslands using burned areas and multivariate logistic regression. International Journal of Remote Sensing **34**(19), 6679–6700. Publisher: Taylor & Francis _eprint: https://doi.org/10.1080/01431161.2013.805280.

Cao, Y., Wang, M. and Liu, K. (2017) Wildfire Susceptibility Assessment in Southern China: A Comparison of Multiple Methods. International Journal of Disaster Risk Science **8**(2), 164–181.

Carrega, P. (1995) A method for the reconstruction of mountain air temperatures with automatic cartographic applications. Theoretical and Applied Climatology **52**(1), 69–84.

Chuvieco, E., Aguado, I., Yebra, M., Nieto, H., Salas, J., Martín, M. P., Vilar, L., Martínez, J., Martín, S., Ibarra, P., de la Riva, J., Baeza, J., Rodríguez, F., Molina, J. R., Herrera, M. A. and Zamora, R. (2010) Development of a framework for fire risk assessment using remote sensing and geographic information system technologies. Ecological Modelling **221**(1), 46–58.

Chuvieco, E., Allgöwer, B. and Salas, J. (2003) Integration of Physical and Human Factors in Fire Danger Assessment. In Wildland Fire Danger Estimation and Mapping, volume

Volume 4 of Series in Remote Sensing, pp. 197–218. WORLD SCIENTIFIC. ISBN 978-981-238-569-7.

Countryman, C. M. (1972) The fire environment concept. Pacific Southwest Forest and Range Experiment Station.

Crespi, A., Matiu, M., Bertoldi, G., Petitta, M. and Zebisch, M. (2020) High-resolution daily series (1980 - 2018) and monthly climatologies (1981 - 2010) of mean temperature and precipitation for Trentino - South Tyrol (north-eastern Italian Alps).

Crespi, A., Matiu, M., Bertoldi, G., Petitta, M. and Zebisch, M. (2021) A high-resolution gridded dataset of daily temperature and precipitation records (1980–2018) for Trentino-South Tyrol (north-eastern Italian Alps). Earth System Science Data **13**(6), 2801–2818. Publisher: Copernicus GmbH.

Deng, J., Wang, W., Gu, G., Chen, Z., Liu, J., Xie, G., Weng, S., Ding, L. and Li, C. (2023) Wildfire susceptibility prediction using a multisource and spatiotemporal cooperative approach. Earth Science Informatics **16**(4), 3511–3529.

Di Giuseppe, F., McNorton, J., Lombardi, A. and Wetterhall, F. (2025) Global data-driven prediction of fire activity. Nature Communications **16**(1), 2918. Publisher: Nature Publishing Group.

Driscoll, D. A., Macdonald, K. J., Gibson, R. K., Doherty, T. S., Nimmo, D. G., Nolan, R. H., Ritchie, E. G., Williamson, G. J., Heard, G. W., Tasker, E. M., Bilney, R., Porch, N., Collett, R. A., Crates, R. A., Hewitt, A. C., Pendall, E., Boer, M. M., Gates, J., Boulton, R. L., Mclean, C. M., Groffen, H., Maisey, A. C., Beranek, C. T., Ryan, S. A., Callen, A., Hamer, A. J., Stauber, A., Daly, G. J., Gould, J., Klop-Toker, K. L., Mahony, M. J., Kelly, O. W., Wallace, S. L., Stock, S. E., Weston, C. J., Volkova, L., Black, D., Gibb, H., Grubb, J. J., McGeoch, M. A., Murphy, N. P., Lee, J. S., Dickman, C. R., Neldner, V. J., Ngugi, M. R., Miritis, V., Köhler, F., Perri, M., Denham, A. J., Mackenzie, B. D. E., Reid, C. A. M., Rayment, J. T., Arriaga-Jiménez, A., Hewins, M. W., Hicks, A., Melbourne, B. A., Davies, K. F., Bitters, M. E., Linley, G. D., Greenville, A. C., Webb, J. K., Roberts, B., Letnic, M., Price, O. F., Walker, Z. C., Murray, B. R., Verhoeven, E. M., Thomsen, A. M., Keith, D., Lemmon, J. S., Ooi, M. K. J., Allen, V. L., Decker, O. T., Green, P. T., Moussalli, A., Foon, J. K., Bryant, D. B., Walker, K. L., Bruce, M. J., Madani, G., Tscharke, J. L., Wagner, B., Nitschke, C. R., Gosper, C. R., Yates, C. J., Dillon, R., Barrett, S., Spencer, E. E., Wardle, G. M., Newsome, T. M., Pulsford, S. A., Singh, A., Roff, A., Marsh, K. J., Mcdonald, K., Howell, L. G., Lane, M. R., Cristescu, R. H., Witt, R. R., Cook, E. J., Grant, F., Law, B. S., Seddon, J., Berris, K. K., Shofner, R. M., Barth, M., Welz, T., Foster, A., Hancock, D., Beitzel, M., Tan, L. X. L., Waddell, N. A., Fallow, P. M., Schweickle, L., Le Breton, T. D., Dunne, C., Green, M., Gilpin, A.-M., Cook, J. M., Power, S. A., Hogendoorn, K., Brawata, R., Jolly, C. J., Tozer, M., Reiter, N. and Phillips, R. D. (2024) Biodiversity impacts of the 2019–2020 Australian megafires. Nature **635**(8040), 898–905. Publisher: Nature Publishing Group.

Eskandari, S., Pourghasemi, H. R. and Tiefenbacher, J. P. (2021) Fire-susceptibility mapping in the natural areas of Iran using new and ensemble data-mining models. Environmental Science and Pollution Research **28**(34), 47395–47406.

European Union's Copernicus Land Monitoring Service information (2020) Tree Cover Density 2018 (raster 10 m), Europe, 3-yearly.

Faivre, N., Jin, Y., Goulden, M. L. and Randerson, J. T. (2014) Controls on the spatial pattern of wildfire ignitions in Southern California. International Journal of Wildland Fire **23**(6), 799–811.

Felsche, E., Böhnisch, A., Poschlod, B. and Ludwig, R. (2024) European hot and dry summers are projected to become more frequent and expand northwards. Communications Earth & Environment **5**(1), 1–11. Publisher: Nature Publishing Group.

Filkov, A. I., Ngo, T., Matthews, S., Telfer, S. and Penman, T. D. (2020) Impact of Australia's catastrophic 2019/20 bushfire season on communities and environment. Retrospective analysis and current trends. Journal of Safety Science and Resilience **1**(1), 44–56.

Finney, M. A. (2005) The challenge of quantitative risk analysis for wildland fire. Forest Ecology and Management **211**(1), 97–108.

Fluss, R., Faraggi, D. and Reiser, B. (2005) Estimation of the Youden Index and its Associated Cutoff Point. Biometrical Journal **47**(4), 458–472. _eprint: https://onlinelibrary.wiley.com/doi/pdf/10.1002/bimj.200410135.

Ganteaume, A., Camia, A., Jappiot, M., San-Miguel-Ayanz, J., Long-Fournel, M. and Lampin, C. (2013) A review of the main driving factors of forest fire ignition over Europe. Environmental Management **51**(3), 651–662.

Ghorbanzadeh, O., Valizadeh Kamran, K., Blaschke, T., Aryal, J., Naboureh, A., Einali, J. and Bian, J. (2019) Spatial Prediction of Wildfire Susceptibility Using Field Survey GPS Data and Machine Learning Approaches. Fire **2**(3), 43. Number: 3 Publisher: Multidisciplinary Digital Publishing Institute.

Giglio, L., Randerson, J. T. and van der Werf, G. R. (2013) Analysis of daily, monthly, and annual burned area using the fourth-generation global fire emissions database (GFED4). Journal of Geophysical Research: Biogeosciences **118**(1), 317–328. _eprint: https://onlinelibrary.wiley.com/doi/pdf/10.1002/jgrg.20042.

Giuseppe, F. D., Pappenberger, F., Wetterhall, F., Krzeminski, B., Camia, A., Libertá, G. and Miguel, J. S. (2016) The potential predictability of fire danger provided by numerical weather prediction. Journal of Applied Meteorology and Climatology **55**(11), 2469–2491. Publisher: American Meteorological Society Section: Journal of Applied Meteorology and Climatology.

de Groot, W. J., Goldammer, J. G., Keenan, T., Brady, M. A., Lynham, T. J., Justice, C. O., Csiszar, I. A. and O'Loughlin, K. (2006) Developing a global early warning system for wildland fire. Forest Ecology and Management **234**, S10.

Guerrero, F., Espinoza, L., Vidal, V., Carmona, C., Krecl, P., Targino, A. C., Ruggeri, M. F. and Toledo, M. (2024) Black carbon and particulate matter concentrations amid central Chile's extreme wildfires. Science of The Total Environment **951**, 175541.

Guzzetti, F., Reichenbach, P., Cardinali, M., Galli, M. and Ardizzone, F. (2005) Probabilistic landslide hazard assessment at the basin scale. Geomorphology **72**(1-4), 272–299. Publisher: Elsevier.

Haiden, T., Kann, A., Wittmann, C., Pistotnik, G., Bica, B. and Gruber, C. (2011) The Integrated Nowcasting through Comprehensive Analysis (INCA) System and Its Validation over the Eastern Alpine Region. Weather and Forecasting **26**(2), 166–183. Publisher: American Meteorological Society.

Hollis, J. J., Matthews, S., Fox-Hughes, P., Grootemaat, S., Heemstra, S., Kenny, B. J. and Sauvage, S. (2024) Introduction to the Australian Fire Danger Rating System†. International Journal of Wildland Fire **33**(3). Publisher: CSIRO PUBLISHING.

Hosmer, D. W., Lemeshow, S. and Sturdivant, R. X. (2013) Applied Logistic Regression: Third Edition. Applied Logistic Regression: Third Edition pp. 1–510. Publisher: wiley.

Jain, P., Coogan, S. C., Subramanian, S. G., Crowley, M., Taylor, S. and Flannigan, M. D. (2020) A review of machine learning applications in wildfire science and management. Environmental Reviews **28**(4), 478–505. Publisher: NRC Research Press.

Jappiot, M., Gonzalez-Olabarria, J. R., Lampin-Maillet, C. and Borgniet, L. (2009) Assessing Wildfire Risk in Time and Space. In Living with wildfires: what science can tell us. A contribution to the Science-Policy Dialogue, pp. 41 – 47. European Forest Institute.

Jellouli, O. and Bernoussi, A. S. (2022) The impact of dynamic wind flow behavior on forest fire spread using cellular automata: Application to the watershed BOUKHALEF (Morocco). Ecological Modelling **468**, 109938.

Jolly, W. M., Cochrane, M. A., Freeborn, P. H., Holden, Z. A., Brown, T. J., Williamson, G. J. and Bowman, D. M. J. S. (2015) Climate-induced variations in global wildfire danger from 1979 to 2013. Nature Communications **6**(1), 7537. Publisher: Nature Publishing Group.

Jones, R. L., Guha-Sapir, D. and Tubeuf, S. (2022) Human and economic impacts of natural disasters: can we trust the global data? Scientific Data **9**(1), 572. Publisher: Nature Publishing Group.

Keeley, J. E. and Syphard, A. D. (2017) Different historical fire–climate patterns in California. International Journal of Wildland Fire **26**(4), 253–268. Publisher: CSIRO PUBLISHING.

Koutsias, N., Allgöwer, B., Kalabokidis, K., Mallinis, G., Balatsos, P. and Goldammer, J. G. (2015) Fire occurrence zoning from local to global scale in the European Mediterranean basin: implications for multi-scale fire management and policy. iForest - Biogeosciences and Forestry **9**(2), 195. Publisher: SISEF - Italian Society of Silviculture and Forest Ecology Section: Modelling.

Kudláčková, L., Bartošová, L., Linda, R., Bláhová, M., Poděbradská, M., Fischer, M., Balek, J., Žalud, Z. and Trnka, M. (2024) Assessing fire danger classes and extreme thresholds of the Canadian Fire Weather Index across global environmental zones: a review. Environmental Research Letters **20**(1), 013001. Publisher: IOP Publishing.

Lemus-Canovas, M., Crespi, A., Maines, E., Terzi, S. and Pittore, M. (2025) More intense heatwaves under drier conditions: a compound event analysis in the Adige River basin (Eastern Italian Alps). Publisher: Copernicus GmbH.

Lemus-Canovas, M., Lopez-Bustins, J. A., Martin-Vide, J. and Royé, D. (2019) synoptReg: An R package for computing a synoptic climate classification and a spatial regionalization of environmental data. Environmental Modelling & Software **118**, 114–119.

Leuenberger, M., Parente, J., Tonini, M., Pereira, M. G. and Kanevski, M. (2018) Wildfire susceptibility mapping: deterministic vs. stochastic approaches. Environmental Modelling & Software **101**, 194–203.

Linn, R., Winterkamp, J., Edminster, C., Colman, J. J. and Smith, W. S. (2007) Coupled influences of topography and wind on wildland fire behaviour. International Journal of Wildland Fire. 16: 183-195. **16**, 183–195.

Lombardo, L., Opitz, T., Ardizzone, F., Guzzetti, F. and Huser, R. (2020) Space-time landslide predictive modelling. Earth-Science Reviews **209**, 103318. Publisher: Elsevier.

Malinowski, R., Lewiński, S., Rybicki, M., Gromny, E., Jenerowicz, M., Krupiński, M., Nowakowski, A., Wojtkowski, C., Krupiński, M., Krätzschmar, E. and Schauer, P. (2020) Automated Production of a Land Cover/Use Map of Europe Based on Sentinel-2 Imagery. Remote Sensing **12**(21), 3523. Number: 21 Publisher: Multidisciplinary Digital Publishing Institute.

Mantero, G., Morresi, D., Negri, S., Anselmetto, N., Lingua, E., Bonifacio, E., Garbarino, M. and Marzano, R. (2023) Short-term drivers of post-fire forest regeneration in the Western Alps. Fire Ecology **19**(1), 23.

Maranghides, A., Link, E., Brown, C. U., Walton, W. D., Mell, W. and Hawks, S. (2023) A Case Study of the Camp Fire - Notification, Evacuation, Traffic, and Temporary Refuge Areas (NETTRA). Technical report, National Institute of Standards and Technology, Gaithersburg, MD. https://doi.org/10.6028/NIST.TN.2252.

Maringer, J., Ascoli, D., Dorren, L., Bebi, P. and Conedera, M. (2016) Temporal trends in the protective capacity of burnt beech forests (Fagus sylvatica L.) against rockfall. European Journal of Forest Research **135**(4), 657–673.

Martin, D. A. and Moody, J. A. (2001) Comparison of soil infiltration rates in burned and unburned mountainous watersheds. Hydrological Processes **15**(15), 2893–2903. _eprint: https://onlinelibrary.wiley.com/doi/pdf/10.1002/hyp.380.

Martínez, J., Vega-Garcia, C. and Chuvieco, E. (2009) Human-caused wildfire risk rating for prevention planning in Spain. Journal of Environmental Management **90**(2), 1241–1252.

McKee, T. B., Doesken, N. J. and Kleist, J. (1993) The relationship of drought frequency and duration of time scales. Eighth Conference on Applied Climatology, American Meteorological Society pp. 179–186.

Moreno, M., Lombardo, L., Crespi, A., Zellner, P. J., Mair, V., Pittore, M., van Westen, C. and Steger, S. (2024) Space-time data-driven modeling of precipitation-induced shallow landslides in South Tyrol, Italy. Science of The Total Environment **912**, 169166.

Moreno, M., Lombardo, L., Steger, S., de Vugt, L., Zieher, T., Crespi, A., Marra, F., van Westen, C. and Opitz, T. (2025) Functional Regression for Space-Time Prediction of Precipitation-Induced Shallow Landslides in South Tyrol, Italy. Journal of Geophysical Research: Earth Surface **130**(4), e2024JF008219. _eprint: https://onlinelibrary.wiley.com/doi/pdf/10.1029/2024JF008219.

Moreno, M., Steger, S., Tanyas, H. and Lombardo, L. (2023) Modeling the area of co-seismic landslides via data-driven models: The Kaikōura example. Engineering Geology **320**, 107121. Publisher: Elsevier.

Moritz, M. A., Morais, M. E., Summerell, L. A., Carlson, J. M. and Doyle, J. (2005) Wildfires, complexity, and highly optimized tolerance. Proceedings of the National Academy of Sciences **102**(50), 17912–17917. Publisher: Proceedings of the National Academy of Sciences.

Müller, M., Vilà Vilardell, L., Vacik, H., Mayer, C., Mayr, S., Carrega, P., Duche, Y., Lahaye, S., Böttcher, F., Maier, H., Schunk, C., Zimmermann, L., Ascoli, D., Cotterchio, A., Fiorucci, P., Gottero, F., Pirone, S., Rizzolo, R., Vacchiano, G. and Sautter, M. (2020a) Forest fires in the Alps - State of knowledge, future challenges and options for an integrated fire management. EUSALP Action Group 8.

Müller, M. M., Vacik, H., Diendorfer, G., Arpaci, A., Formayer, H. and Gossow, H. (2013) Analysis of lightning-induced forest fires in Austria. Theoretical and Applied Climatology **111**(1), 183–193.

Müller, M. M., Vilà-Vilardell, L. and Vacik, H. (2020b) Towards an integrated forest fire danger assessment system for the European Alps. Ecological Informatics **60**, 101151.

NASA JPL (2020) NASADEM Merged DEM Global 1 arc second V001.

Noble, I. R., Gill, A. M. and Bary, G. a. V. (1980) McArthur's fire-danger meters expressed as equations. Australian Journal of Ecology **5**(2), 201–203. _eprint: https://onlinelibrary.wiley.com/doi/pdf/10.1111/j.1442-9993.1980.tb01243.x.

Norbiato, D., Borga, M., Merz, R., Blöschl, G. and Carton, A. (2009) Controls on event runoff coefficients in the eastern Italian Alps. Journal of Hydrology **375**(3), 312–325.

Oliveira, S., Gonçalves, A. and Zêzere, J. L. (2021) Reassessing wildfire susceptibility and hazard for mainland Portugal. Science of The Total Environment **762**, 143121.

Oliveira, S., Moreira, F., Boca, R., San-Miguel-Ayanz, J. and Pereira, J. M. C. (2013) Assessment of fire selectivity in relation to land cover and topography: a comparison between Southern European countries. International Journal of Wildland Fire **23**(5), 620–630. Publisher: CSIRO PUBLISHING.

Oliveira, S., Oehler, F., San-Miguel-Ayanz, J., Camia, A. and Pereira, J. M. C. (2012) Modeling spatial patterns of fire occurrence in Mediterranean Europe using Multiple Regression and Random Forest. Forest Ecology and Management **275**, 117–129.

Oliveras, I., Gracia, M., Moré, G. and Retana, J. (2009) Factors influencing the pattern of fire severities in a large wildfire under extreme meteorological conditions in the Mediterranean basin. International Journal of Wildland Fire **18**(7), 755–764. Publisher: CSIRO PUBLISHING.

OpenStreetMap contributors (2017) Planet dump retrieved from https://planet.osm.org. Published: https://www.openstreetmap.org.

Opitz, T., Bakka, H., Huser, R. and Lombardo, L. (2022) High-resolution Bayesian mapping of landslide hazard with unobserved trigger event. The Annals of Applied Statistics **16**(3), 1653–1675. Publisher: Institute of Mathematical Statistics.

Pagnon Eriksson, C., Johansson, N. and McNamee, M. (2023) The performance of wildfire danger indices: A Swedish case study. Safety Science **159**, 106038.

Parente, J. and Pereira, M. G. (2016) Structural fire risk: The case of Portugal. Science of The Total Environment **573**, 883–893.

Patton, A. I., Luna, L. V., Roering, J. J., Jacobs, A., Korup, O. and Mirus, B. B. (2023) Landslide initiation thresholds in data-sparse regions: application to landslide early warning criteria in Sitka, Alaska, USA. Natural Hazards and Earth System Sciences **23**(10), 3261–3284. Publisher: Copernicus GmbH.

Pittore, M., Campalani, P., Renner, K., Plörer, M. and Tagliavini, F. (2023) Border-independent multi-functional, multi-hazard exposure modelling in Alpine regions. Natural Hazards **119**(2), 837–858.

Pourtaghi, Z. S., Pourghasemi, H. R., Aretano, R. and Semeraro, T. (2016) Investigation of general indicators influencing on forest fire and its susceptibility modeling using different data mining techniques. Ecological Indicators **64**, 72–84.

Povak, N. A., Hessburg, P. F. and Salter, R. B. (2018) Evidence for scale-dependent topographic controls on wildfire spread. Ecosphere **9**(10), e02443. _eprint: https://onlinelibrary.wiley.com/doi/pdf/10.1002/ecs2.2443.

Pyne, S. J., Andrews, P. L. and Laven, R. D. (1996) Introduction to wildland fire. Second edition. New York, USA: John Wiley and Sons. ISBN 978-0-471-54913-0.

Pérez-Sánchez, J., Senent-Aparicio, J., Díaz-Palmero, J. M. and Cabezas-Cerezo, J. d. D. (2017) A comparative study of fire weather indices in a semiarid south-eastern Europe region. Case of study: Murcia (Spain). Science of The Total Environment **590-591**, 761–774.

Renner, K., Schneiderbauer, S., Pruß, F., Kofler, C., Martin, D. and Cockings, S. (2018) Spatio-temporal population modelling as improved exposure information for risk assessments tested in the Autonomous Province of Bolzano. International Journal of Disaster Risk Reduction **27**, 470–479.

Richards, J., Huser, R., Bevacqua, E. and Zscheischler, J. (2023) Insights into the drivers and spatiotemporal trends of extreme Mediterranean wildfires with statistical deep learning. Artificial Intelligence for the Earth Systems **2**(4). Publisher: American Meteorological Society Section: Artificial Intelligence for the Earth Systems.

Richardson, D., Black, A. S., Irving, D., Matear, R. J., Monselesan, D. P., Risbey, J. S., Squire, D. T. and Tozer, C. R. (2022) Global increase in wildfire potential from compound fire weather and drought. npj Climate and Atmospheric Science **5**(1), 1–12. Publisher: Nature Publishing Group.

Robichaud, P. R. and Elliot, W. J. (2006) Protection from erosion following wildfire. Unpublished paper written for presentation at the 2006 ASABE Annual International Meeting, Portland Convention Center, Portland, OR, July 9-12, 2006. ASABE Paper No. 068009. St. Joseph, MI: American Society of Agricultural and Biological Engineers. 7 p .

Rotbarth, R., van Nes, E. H., Scheffer, M. and Holmgren, M. (2025) Boreal forests are heading for an open state. Proceedings of the National Academy of Sciences **122**(2), e2404391121. Publisher: Proceedings of the National Academy of Sciences.

Ruffault, J., Curt, T., Moron, V., Trigo, R. M., Mouillot, F., Koutsias, N., Pimont, F., Martin-StPaul, N., Barbero, R., Dupuy, J.-L., Russo, A. and Belhadj-Khedher, C. (2020) Increased likelihood of heat-induced large wildfires in the Mediterranean Basin. Scientific Reports **10**(1), 13790. Publisher: Nature Publishing Group.

Ruopp, M. D., Perkins, N. J., Whitcomb, B. W. and Schisterman, E. F. (2008) Youden Index and Optimal Cut-Point Estimated from Observations Affected by a Lower Limit of Detection. Biometrical journal. Biometrische Zeitschrift **50**(3), 419–430.

Ríos-Pena, L., Kneib, T., Cadarso-Suárez, C. and Marey-Pérez, M. (2017) Predicting the occurrence of wildfires with binary structured additive regression models. Journal of Environmental Management **187**, 154–165.

Saito, T. and Rehmsmeier, M. (2015) The Precision-Recall Plot Is More Informative than the ROC Plot When Evaluating Binary Classifiers on Imbalanced Datasets. PLOS ONE **10**(3), e0118432. Publisher: Public Library of Science.

de Santana, R. O., Delgado, R. C. and Schiavetti, A. (2021) Modeling susceptibility to forest fires in the Central Corridor of the Atlantic Forest using the frequency ratio method. Journal of Environmental Management **296**, 113343.

Santos, R., Russo, A. and Gouveia, C. M. (2024) Co-occurrence of marine and atmospheric heatwaves with drought conditions and fire activity in the Mediterranean region. Scientific Reports **14**(1), 19233. Publisher: Nature Publishing Group.

Sass, O., and Sarcletti, S. (2017) Patterns of long-term regeneration of forest fire slopes in the Northern European Alps – a logistic regression approach. Geografiska Annaler: Series A, Physical Geography **99**(1), 56–71. Publisher: Taylor & Francis _eprint: https://doi.org/10.1080/04353676.2016.1263131.

Schlögl, M., Spiekermann, R. and Steger, S. (2025) Towards a holistic assessment of landslide susceptibility models: insights from the Central Eastern Alps. Environmental Earth Sciences **84**(4), 113.

Schunk, C., Wastl, C., Leuchner, M., Schuster, C. and Menzel, A. (2013) Forest fire danger rating in complex topography – results from a case study in the Bavarian Alps in autumn 2011. Natural Hazards and Earth System Sciences **13**(9), 2157–2167. Publisher: Copernicus GmbH.

Scott, J., Helmbrecht, D., Thompson, M. P., Calkin, D. E. and Marcille, K. (2012) Probabilistic assessment of wildfire hazard and municipal watershed exposure. Natural Hazards **64**(1), 707–728.

Sebastián-López, A., Salvador-Civil, R., Gonzalo-Jiménez, J. and SanMiguel-Ayanz, J. (2008) Integration of socio-economic and environmental variables for modelling long-term fire danger in Southern Europe. European Journal of Forest Research **127**(2), 149–163.

Sirca, C., Salis, M., Arca, B., Duce, P. and Spano, D. (2018) Assessing the performance of fire danger indexes in a Mediterranean area. iForest - Biogeosciences and Forestry **11**(5), 563. Publisher: SISEF - Italian Society of Silviculture and Forest Ecology Section: Forest Dynamics and Natural Disturbances.

Smith, J. T., Allred, B. W., Boyd, C. S., Davies, K. W., Jones, M. O., Kleinhesselink, A. R., Maestas, J. D. and Naugle, D. E. (2023) Where There's Smoke, There's Fuel: Dynamic Vegetation Data Improve Predictions of Wildfire Hazard in the Great Basin. Rangeland Ecology & Management **89**, 20–32.

Song, H.-S., and Lee, S.-H. (2017) Effects of wind and tree density on forest fire patterns in a mixed-tree species forest. Forest Science and Technology **13**(1), 9–16. Publisher: Taylor & Francis _eprint: https://doi.org/10.1080/21580103.2016.1262793.

Steger, S., Moreno, M., Crespi, A., Luigi Gariano, S., Teresa Brunetti, M., Melillo, M., Peruccacci, S., Marra, F., de Vugt, L., Zieher, T., Rutzinger, M., Mair, V. and Pittore, M. (2024) Adopting the margin of stability for space–time landslide prediction – A data-driven approach for generating spatial dynamic thresholds. Geoscience Frontiers **15**(5), 101822.

Steger, S., Moreno, M., Crespi, A., Zellner, P. J., Gariano, S. L., Brunetti, M. T., Melillo, M., Peruccacci, S., Marra, F., Kohrs, R., Goetz, J., Mair, V. and Pittore, M. (2023) Deciphering seasonal effects of triggering and preparatory precipitation for improved shallow landslide prediction using generalized additive mixed models. Natural Hazards and Earth System Sciences **23**(4), 1483–1506. Publisher: Copernicus GmbH.

Tonini, M., D'Andrea, M., Biondi, G., Degli Esposti, S., Trucchia, A. and Fiorucci, P. (2020) A Machine Learning-Based Approach for Wildfire Susceptibility Mapping. The Case Study of the Liguria Region in Italy. Geosciences **10**(3), 105. Number: 3 Publisher: Multidisciplinary Digital Publishing Institute.

Trucchia, A., Izadgoshasb, H., Isnardi, S., Fiorucci, P. and Tonini, M. (2022a) Machine-learning applications in geosciences: comparison of different algorithms and vegetation classes' importance ranking in wildfire susceptibility. Geosciences **12**(11), 424. Number: 11 Publisher: Multidisciplinary Digital Publishing Institute.

Trucchia, A., Meschi, G., Fiorucci, P., Gollini, A. and Negro, D. (2022b) Defining wildfire susceptibility maps in Italy for understanding seasonal wildfire regimes at the national level. Fire **5**(1), 30. Number: 1 Publisher: Multidisciplinary Digital Publishing Institute.

Turco, M., von Hardenberg, J., AghaKouchak, A., Llasat, M. C., Provenzale, A. and Trigo, R. M. (2017) On the key role of droughts in the dynamics of summer fires in Mediterranean Europe. Scientific Reports **7**(1), 81. Publisher: Nature Publishing Group.

Turco, M., Jerez, S., Doblas-Reyes, F. J., AghaKouchak, A., Llasat, M. C. and Provenzale, A. (2018) Skilful forecasting of global fire activity using seasonal climate predictions. Nature Communications **9**(1), 2718. Publisher: Nature Publishing Group.

Verde, J. C. and Zêzere, J. L. (2010) Assessment and validation of wildfire susceptibility and hazard in Portugal. Natural Hazards and Earth System Sciences **10**(3), 485–497. Publisher: Copernicus GmbH.

Vicente-Serrano, S. M., Beguería, S. and López-Moreno, J. I. (2010) A Multiscalar Drought Index Sensitive to Global Warming: The Standardized Precipitation Evapotranspiration Index. Journal of Climate **23**(7), 1696–1718.

Viegas, D. X., Bovio, G., Ferreira, A., Nosenzo, A. and Sol, B. (1999) Comparative study of various methods of fire danger evaluation in southern Europe. International Journal of Wildland Fire **9**(4), 235–246. Publisher: CSIRO PUBLISHING.

Wagner, V. and E, C. (1987) Development and structure of the Canadian Forest Fire Weather Index System. ISBN 978-0-662-15198-2. ISSN: None.

Wastl, C., Schunk, C., Leuchner, M., Pezzatti, G. B. and Menzel, A. (2012) Recent climate change: Long-term trends in meteorological forest fire danger in the Alps. Agricultural and Forest Meteorology **162-163**, 1–13.

van der Werf, G. R., Randerson, J. T., Giglio, L., van Leeuwen, T. T., Chen, Y., Rogers, B. M., Mu, M., van Marle, M. J. E., Morton, D. C., Collatz, G. J., Yokelson, R. J. and Kasibhatla, P. S. (2017) Global fire emissions estimates during 1997–2016. Earth System Science Data **9**(2), 697–720. Publisher: Copernicus GmbH.

Wood, S. N. (2006) Generalized Additive Models : An introduction with R. New York: Chapman and Hall/CRC. Publication Title: Generalized Additive Models.

Wood, S. N. (2017) Generalized Additive Models: An Introduction with R, Second Edition. Second edition. New York: Chapman and Hall/CRC. ISBN 978-1-315-37027-9.

Woolford, D. G., Bellhouse, D. R., Braun, W. J., Dean, C. B., Martell, D. L. and Sun, J. (2011) A spatio-temporal model for people-caused forest fire occurrence in the Romeo Malette Forest. Journal of Environmental Statistics **2**(1), 26.

Yue, W., Ren, C., Liang, Y., Liang, J., Lin, X., Yin, A. and Wei, Z. (2023) Assessment of Wildfire Susceptibility and Wildfire Threats to Ecological Environment and Urban Development Based on GIS and Multi-Source Data: A Case Study of Guilin, China. Remote Sensing **15**(10), 2659. Number: 10 Publisher: Multidisciplinary Digital Publishing Institute.

Zhang, G., Wang, M. and Liu, K. (2021) Deep neural networks for global wildfire susceptibility modelling. Ecological Indicators **127**, 107735.

Zscheischler, J., Westra, S., van den Hurk, B. J. J. M., Seneviratne, S. I., Ward, P. J., Pitman, A., AghaKouchak, A., Bresch, D. N., Leonard, M., Wahl, T. and Zhang, X. (2018) Future climate risk from compound events. Nature Climate Change **8**(6), 469–477. Publisher: Nature Publishing Group.

Zuur, A. F., Ieno, E. N., Walker, N., Saveliev, A. A. and Smith, G. M. (2009) Mixed effects models and extensions in ecology with R. Statistics for Biology and Health. New York, NY: Springer New York.